SPACEINN WP4 Helioseismology
Deliverable D4.10
Report on local helioseismology working group meeting #2

Coordinated by Max-Planck-Institut für Sonnensystemforschung (MPG)

The second SPACEINN local helioseismology working group meeting was held at Max-Planck-Institut für Sonnensystemforschung in Göttingen, Germany, on 4 September, 2014.

Purpose of the SPACEINN local helioseismology working group meeting:

One of the goals of SPACEINN WP4 project is to collect all available information about sources of systematic effects, some of which are known to a few instrument scientists or experts in data analysis, but not accessible to the broader community. This group meeting is for presentations and discussions for known systematics.

Programme:

SPACEINN local helioseismology working group meeting: Systematics

Chair: Kaori Nagashima(MPG)

September 4, 2014		
9:00 - 9:30	**Sylvain Korzennik** (Harvard-Smithsonian Center for Astrophysics)	What can we learn about the solar subsurface large scale flows from accurate high-degree modes frequencies?
9:30 - 10:00	**Thomas L. Duvall Jr.** (MPG)	A new time-distance measurement of meridional circulation that is not susceptible to center-to-limb effects
10:00 - 10:40	Coffee break	
10:40 - 11:00	**Timothy Larson** (Stanford University)	Medium-degree analysis of Mount Wilson data
11:00 – 11:20	**Kaori Nagashima** (MPG)	SDO/HMI multi-height velocity measurements
11:20 - 11:40	**Vincent Böning** (KIS)	Extension to spherical geometry: sensitivity kernels for flows in time-distance helioseismology
11:40 - 12:00	**Ariane Schad** (KIS)	Distortion of global mode eigenfunctions

Some photos of the meeting

At the beginning, the chair is explaining the purpose of the meeting.

T. Duvall is giving a talk.

T. Larson is giving a talk.

Participants:

Antia, H.M. (Tata Institute of Fundamental Research)
Appourchaux, Thierry (UPS IAS)
Ayukov, Sergey (Moscow State University)
Baker, David M. (MPG)
Barekat, Atefeh (MPG)
Ball, Warrick (Georg-August-Universität Göttingen)
Baturin, Vladimir (Moscow State University)
Baudin, Frédéric (UPS IAS)
Bhattacharya, Jishnu (Tata Institute of Fundamental Research)
Birch, Aaron (MPG)
Bogart, Richard (Stanford University)
Böning, Vincent (KIS)
Brandenburg, Axel (NORDITA)
Braun, Douglas (NorthWest Research Associates)
Broomhall, Anne-Marie (University of Warwick)
Cally, Paul (Monash University)
Cameron, Robert (MPG)
Davies, Guy (University of Birmingham)
Duvall, Jr., Thomas L. (MPG)
Fleck, Bernhard (ESA)
Fournier, Damien (Georg-August- Universität Göttingen)
Gangadharan, Vigeesh (KIS)
Garcia, Rafael A.(CEA)
Gizon, Laurent (MPG)
Glogowski, Kolja (KIS)
Hanasoge, Shravan (Tata Institute of Fundamental Research)
Hill, Frank (AURA NSO)
Holzwarth, Volkmar (KIS)
Howe, Rachel (University of Birmingham)
Ilonidis, Stathis (Stanford University)
Kiefer, René (KIS)
Komm, Rudolf (AURA NSO)
Korzennik, Sylvain (Harvard-Smithsonian Center for Astrophysics)
Küker, Manfred (Leibniz Institute for Astrophysics Potsdam)
Langfellner, Jan (Georg-August- Universität Göttingen/MPG)
Larson, Timothy (Stanford University)

Leibacher, John (AURA NSO)
Lindsey, Charles (NorthWest Research Associates)
Löptien, Björn (Georg-August- Universität Göttingen/MPG)
Losada, Illa (NORDITA)
Moradi, Hamed (Monash University)
Nagashima, Kaori (MPG)
Papini, Emanuele (MPG)
Patrón, Jesús (IAC)
Przybylski, Damien (Monash University)
Rabello Soares, Maria-Cristina (Universidade Federal de Minas Gerais)
Reinhold, Timo (Georg-August- Universität Göttingen)
Rhodes, Edward (University of Southern California)
Rijs, Carlos (Monash University)
Roth, Markus (KIS)
Rüdiger, Günther (Leibniz Institute for Astrophysics Potsdam)
Schad, Ariane (KIS)
Scherrer, Phil (Stanford University)
Schou, Jesper (MPG)
Schunker, Hannah (MPG)
Sekii, Takashi (National Astronomical Observatory of Japan)
Shelyag, Sergiy (Monash University)
Singh, Nishant K. (NORDITA)
Sreenivasan, Katepalli (New York University Polytechnic School of Engineering)
Suarez Sola, Igor (AURA/NSO)
Švanda, Michal (Astronomical Institute, Academy of Sciences of the Czech Republic)
Thompson, Michael (UCAR/HAO)
Tripathy, Sushanta C. (AURA/NSO)
Turck-Chièze, Sylvaine (CEA)
Vorontsov, Sergei (Queen Mary University of London)
Warnecke, Jörn (MPG)
Wisniewska, Aneta (KIS)
Zhao, Junwei (Stanford University)

Outcome of the meeting:

Based on the talks of the meeting and the personal discussions between the participants of the meeting, we have set up a website where anyone can access information about sources of systematic effects of observation datasets related to helioseismology analysis. We will keep collecting the information and will update the information when needed. (The final version of this website will become a part of Deliverable D4.13 "Report on systematic effects")

The website about the systematics:

http://www2.mps.mpg.de/projects/seismo/SpaceInn/systematics.html

Link to this webpage is available from the "Observations" button on SPACEINN WP4 Local Helioseismology top page.

Screenshot of the website:

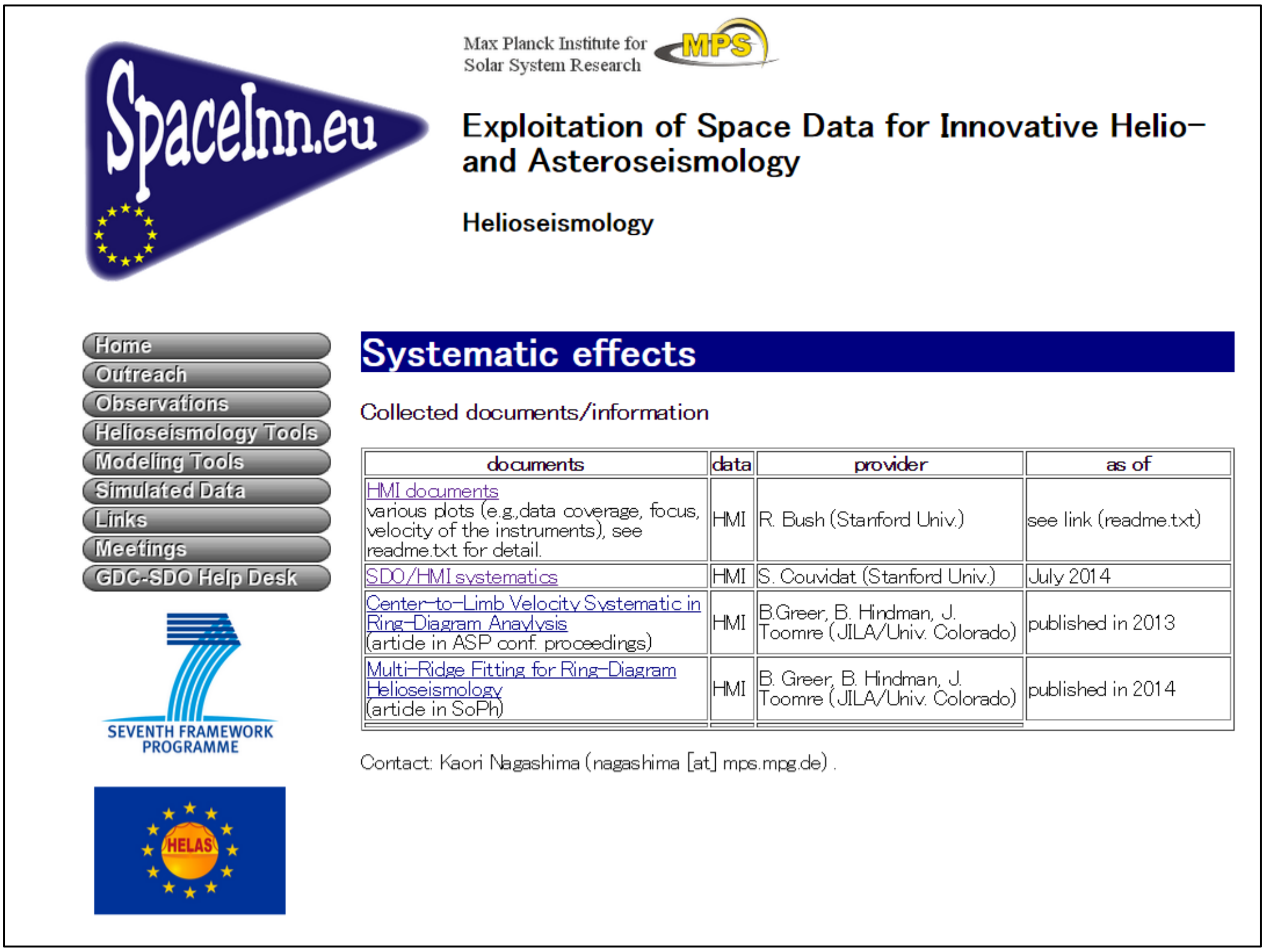

Max Planck Institute for Solar System Research

Exploitation of Space Data for Innovative Helio- and Asteroseismology

Helioseismology

Home
Outreach
Observations
Helioseismology Tools
Modeling Tools
Simulated Data
Links
Meetings
GDC-SDO Help Desk

Systematic effects

Collected documents/information

documents	data	provider	as of
HMI documents various plots (e.g.,data coverage, focus, velocity of the instruments), see readme.txt for detail.	HMI	R. Bush (Stanford Univ.)	see link (readme.txt)
SDO/HMI systematics	HMI	S. Couvidat (Stanford Univ.)	July 2014
Center-to-Limb Velocity Systematic in Ring-Diagram Analysis (article in ASP conf. proceedings)	HMI	B.Greer, B. Hindman, J. Toomre (JILA/Univ. Colorado)	published in 2013
Multi-Ridge Fitting for Ring-Diagram Helioseismology (article in SoPh)	HMI	B. Greer, B. Hindman, J. Toomre (JILA/Univ. Colorado)	published in 2014

Contact: Kaori Nagashima (nagashima [at] mps.mpg.de) .

SEVENTH FRAMEWORK PROGRAMME

HELAS

Appendix

Presentations at the meeting

1. Sylvain Korzennik (Harvard-Smithsonian Center for Astrophysics)	What can we learn about the solar subsurface large scale flows from accurate high-degree modes frequencies?
2. Thomas L. Duvall Jr. (MPG)	A new time-distance measurement of meridional circulation that is not susceptible to center-to-limb effects
3. Timothy Larson (Stanford University)	Medium-degree analysis of Mount Wilson data
4. Kaori Nagashima (MPG)	SDO/HMI multi-height velocity measurements
5. Vincent Böning (KIS)	Extension to spherical geometry: sensitivity kernels for flows in time-distance helioseismology
6. Ariane Schad (KIS)	Distortion of global mode eigenfunctions
7. Richard Bogart * (Stanford University)	HMI Local Helioseismology Data: Status and Prospects

* Richard Bogart was a participant of the meeting, and we discussed with him about the systematics. Here we attached his document about the systematics as well.

1. Sylvain Korzennik

What Can We Learn about the Solar Subsurface Large Scale Flows from Accurate High-Degree Modes Frequencies?

Helas VI — SOHO 28 — SPACEINN
Göttingen, GE

S.G. Korzennik

Harvard-Smithsonian Center for Astrophysics, USA.

September 2014

Contributors: A. Eff-Darwich (ULL, IAC)
T. Larson (Stanford)
M.C. Rabello-Soares (UFMG)
J. Schou (MPS)

Introduction

- High degrees “problem”:
  - modes blend into ridges ($\ell > 200$, for p-modes, $\ell > 300$ for f-modes),
  - ridge characteristics (ν, A, Γ, α) are *not* the mode characteristics.
- Methodology
  - Fit ridges ($100 \le \ell \le 1000$),
  - Use multi-taper estimator (to reduce realization noise).
  - Apply a ridge to mode correction, based on *best* possible model of mode blending - dominated by the *effective* leakage matrix.
  - Iterate on model input parameters to best match observations.
  - Use the $100 \le \ell \le 300$ overlap for validation.

Coverage in the (ℓ, ν) Plane

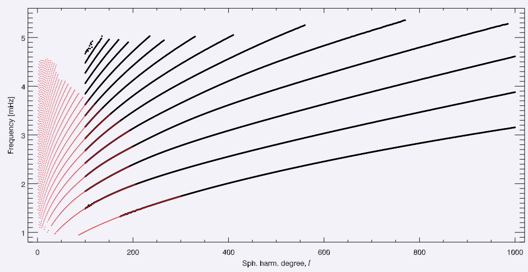

- Red dots: low and intermediate degrees: fitting resolved modes.
- Black circles: high degrees modes: ridge fitting.

Data Sets Analyzed

	2001 90 day long	2002 98 day long	2010 67 day long
MDI	√	√	√
GONG		√	√
HMI			√

- All epochs correspond to MDI *Dynamics* epochs.
- Can extend the time series for HMI & GONG.

Comparison with Resolved Modes

Year	Instrument	$\Delta\nu$ [μHz]	$\Delta\nu/\sigma_\nu$
2001	MDI	-0.220 ± 0.673	-0.880 ± 2.182
2002	MDI	-0.298 ± 0.966	-0.862 ± 2.631
	GONG	0.176 ± 0.769	0.517 ± 2.416
2010	MDI	-0.088 ± 1.087	-0.077 ± 2.766
	GONG	0.748 ± 1.186	2.751 ± 2.411
	HMI	0.269 ± 0.616	0.880 ± 2.044

- Mean and standard deviation of
  - frequency differences, and
  - frequency differences normalized by their uncertainties,

  between estimated mode frequencies derived from ridge fitting and coeval resolved mode frequencies measurements,
- for the $100 \le \ell \le 200|300$ overlapping range.

Comparison with Resolved Modes (cont’d)

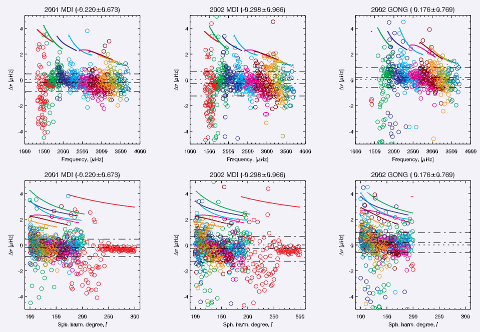

- Circles: frequency differences; dots: ridge to mode correction
- Differences are small, clustered near zero, with no discernible trends, and much smaller than the correction itself.
- The largest scatter is seen for the f-mode below $\ell = 250$ or so.

Comparison with Resolved Modes (cont'd)

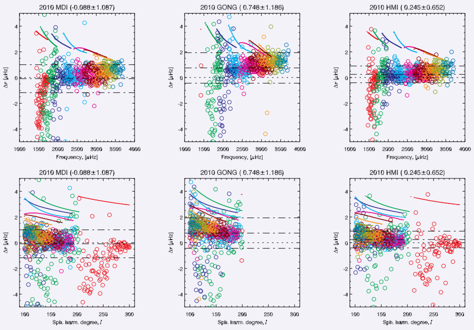

- Similar plot for MDI, GONG and HMI 2010.
- GONG comparison shows a larger bias (2.8σ)
- Scatter for the f-mode remains large even above $\ell = 250$.
- Is this the result of using a shorter time series? (67 versus 90 or 98 days).

Comparison at High Degree between Data Sets

Year	Instruments	$\Delta\nu$ [μHz]	$\Delta\nu/\sigma_\nu$
2002	GONG − MDI	-0.222 ± 0.460	-1.317 ± 1.470
2010	GONG − MDI	-0.982 ± 0.934	-4.260 ± 2.770
	HMI − MDI	-0.655 ± 1.117	-2.162 ± 1.572

- Mean and standard deviation of
  - frequency differences, and
  - frequency differences normalized by their uncertainties,
- between estimated mode frequencies derived from ridge fitting for different instruments and coeval epochs, with respect to MDI values.

Comparison of ν, Γ, & α, 2002

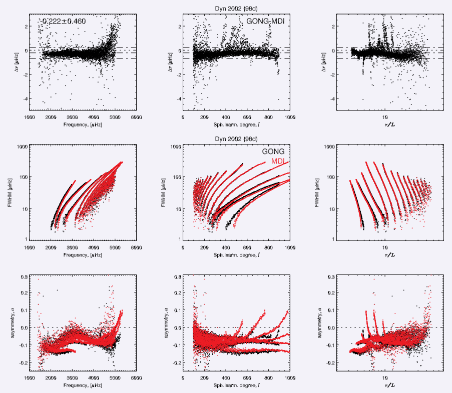

Comparison of ν, Γ, & α, 2010

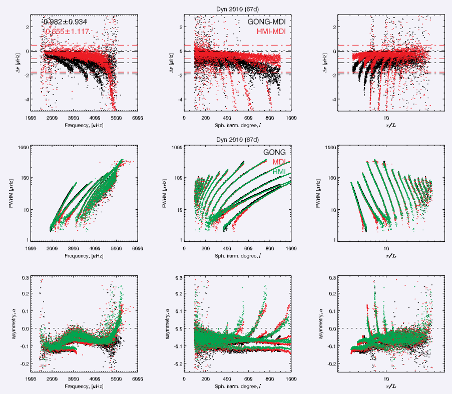

- By contrast with the 2002 data, the frequency comparison shows a variation with degree, and some dependence on frequency.

Comparison of Clebsch–Gordan Coefficients

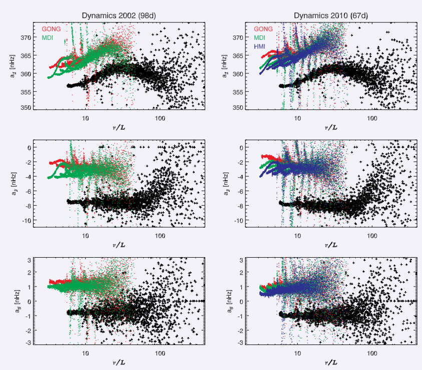

- Color dots: coefficients derived from ridge fitting.
- Black crosses: coefficients derived from coeval resolved mode fitting.

⇒ Large offset between ridge and mode estimate, and between instruments.

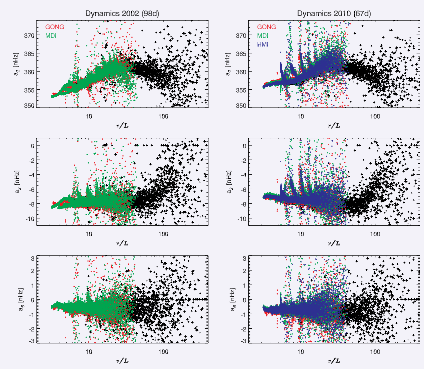

- Color circles: coefficients derived from mode estimates, after correcting ridge fitting results.
- Black crosses: coefficients derived from coeval resolved mode fitting.

⇒ Despite *horns*, both the offset high degree and mode estimate, and between instruments has vanished - no *ad hoc* fudging.

Rotation Inversions

- Inversion model grid (semi uniform in radius and latitude),
- shown in cartesian coordinates.

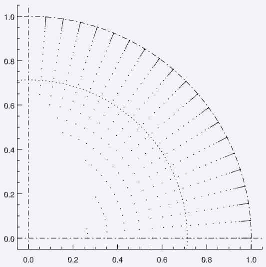

- A. Eff-Darwich inversion method.

Averaging Kernels

- Kernels for inversions using or not high degree modes (left vs right)

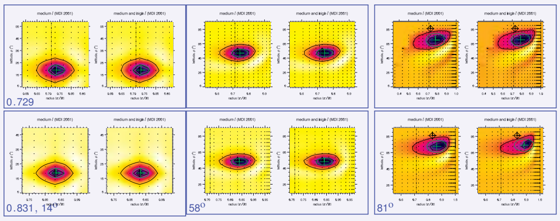

- Target location: black cross-diamond symbols,
- Kernel center of gravity and width: green crosses and circles.
- Inversion grid: black dots.

Averaging Kernels (Cont'd)

- Top 10%

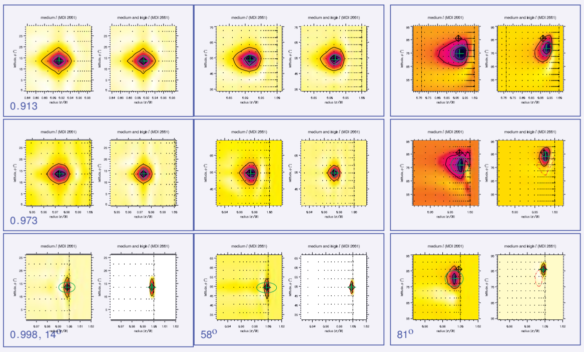

- Ratio of Γ_{ak} and differences Λ,
- for rotation inversions using or not high degree modes.

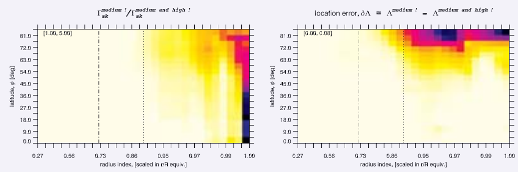

$$\Gamma_{ak} = \int K_a^2(r,\phi) D^2(r,\phi) dr d\phi \Big/ \int K_a^2(r,\phi) dr d\phi$$

$$\Lambda^2 = (r_t - r_c)^2 + ((\phi_t - \phi_c)/(\pi/2))^2$$

where $D^2 = (r - r_c)^2 + ((\phi - \phi_c)/(\pi/2))^2$, and (r_c, ϕ_c) is an estimate of the center of gravity of the averaging kernel main peak; and (r_t, ϕ_t) is the inversion target location on the solution grid.

Rotation Rate in the Outer 10% of the Solar Interior

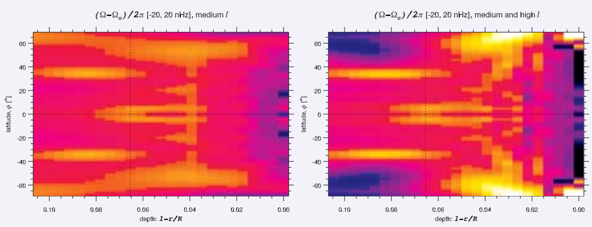

- after subtracting a differential rotation profile, inferred using or not high degree modes (right and left panels).

Note

- (a) the "torsonial oscillations" signal stands out more clearly when including high degrees, and
- (b) the profiles are quite different in the top 5%, esp. at high latitudes.

Medium-ℓ Only

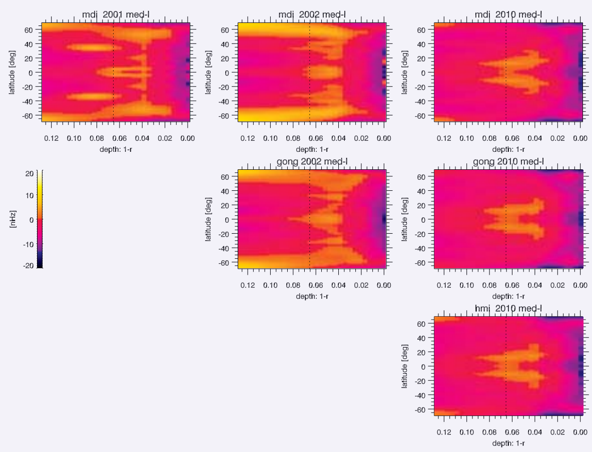

High- and Medium-ℓ

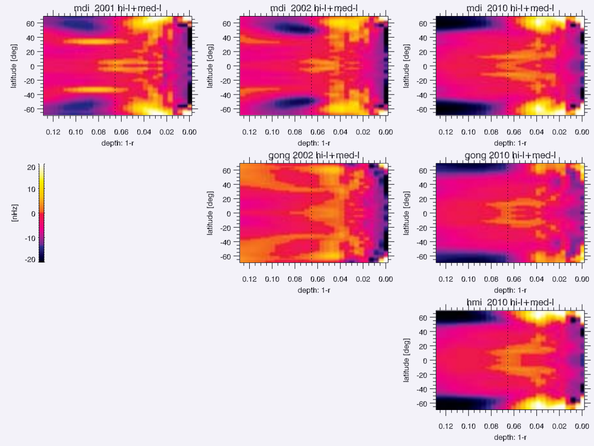

Conclusions

- Can use ridge values to estimate mode parameter.
- Discrepancies remains, likely due to short time series, error in PSF, ...
- GONG, MDI & HMI overlap can be leveraged to resolve this.
- Inclusion of high degree splittings affects solution in the top 10%, and alters the solution in the top 5%.
- Should produce and use high-degree mode estimates on a regular basis.

Tables are available at
`https://www.cfa.harvard.edu/~sylvain/research/`
under
`https://www.cfa.harvard.edu/~sylvain/research/tables/HiL/`

The End

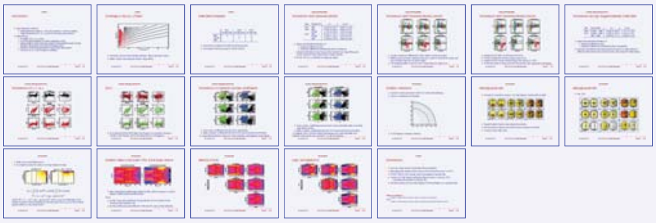

2. Thomas L. Duvall Jr.

Time-distance measurements of meridional circulation using pairs of points at equal center-to-limb angle

Tom Duvall

Deep Chakraborty

Tim Larsen

Examples of ray paths for measuring meridional circulation (left); expected travel-time differences for a single radial cell model (right)

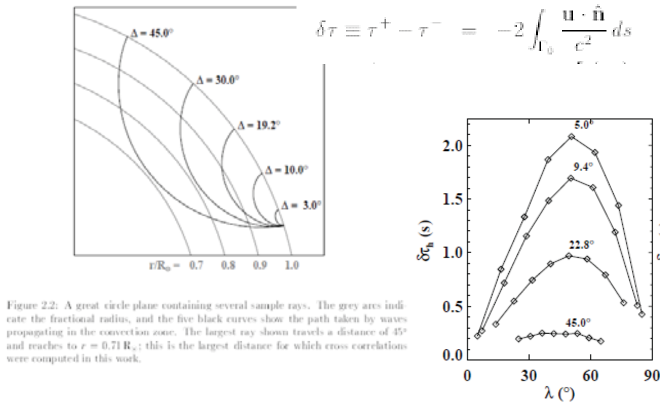

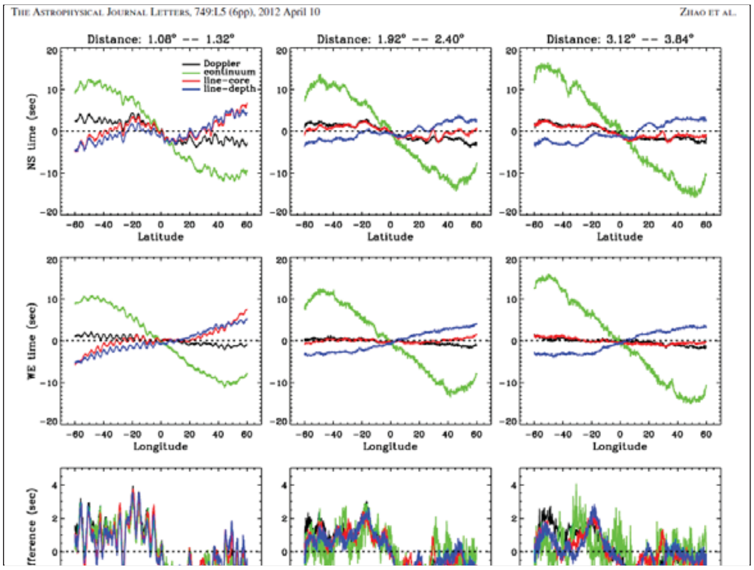

The problem: east-west signal very similar to north-south

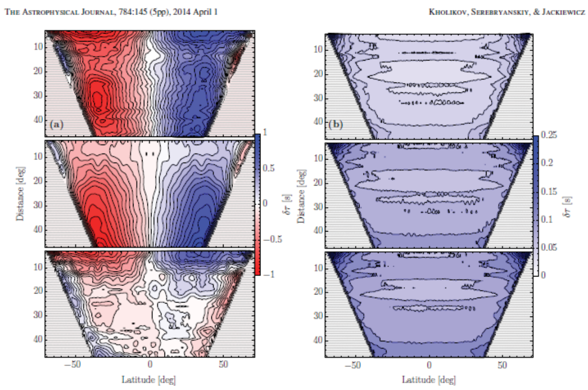

Figure 2. Travel-time difference maps obtained using 652 daily sets of Doppler velocity images. Column (a) shows the S-N, E-W, and S-NE-W contour maps from top to bottom, respectively. Column (b) plots the corresponding measurement uncertainties associated with each panel in column (a). Note the x-axis in the middle panel in each column is the longitude, with the same numerical scale values as shown for latitude (±75°). Hatched regions show where no measurements were computed due to limb constraints.

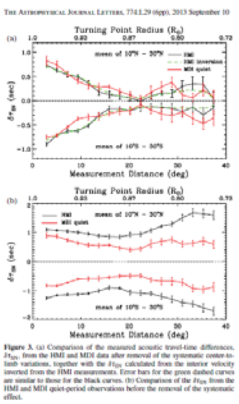

Geometry for measurement technique

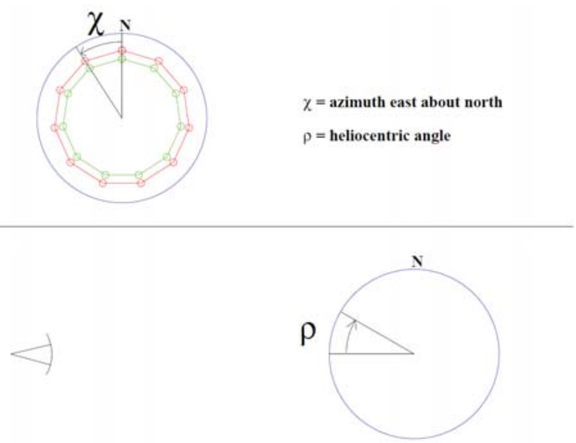

Analysis steps:

- 1) each HMI image is put onto a longitude-sin(latitude) cooordinate system (Tim)
- 2) Spherical harmonics computed for l<=300 (Tim)
- 3) Images reconstructed on azimuth-heliocentric angle coordinate system for 1 year. This involves putting b0 back in. (Tom, Deep, Tim, Shukur)
- 4) Filtering is done only as a 1st difference in time. (Tom)
- 5) Cross correlations for each day for different lags in azimuth and at the different heliocentric angles separately.
- 6) Average correlations over 1 year.
- 7) Travel times computed using the Gizon-Birch method. A separate reference cross correlation is computed for each heliocentric angle.
- 8) Travel time differences are computed for oppositely directed waves.
- 9) Symmetric and antisymmetric components about the central meridian to separate rotation and meridional circulation.

Polynomial fit to travel time vs. azimuth

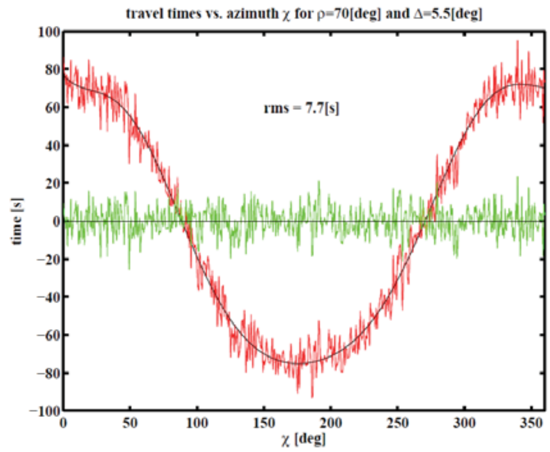

Symmetric and antisymmetric parts (across central meridian)

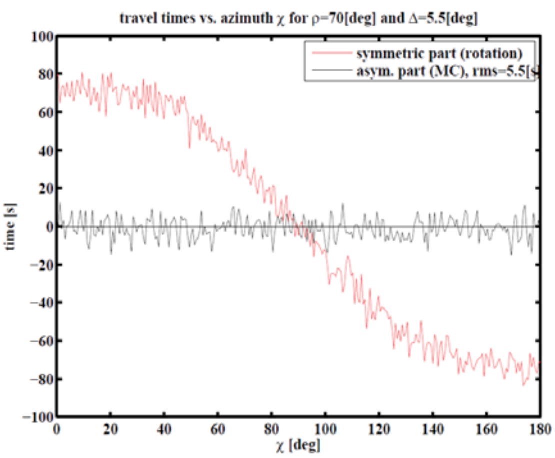

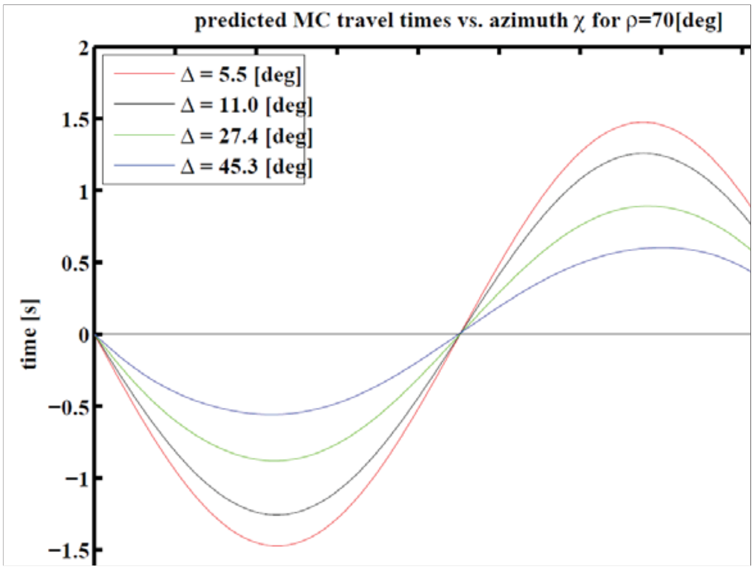

Summary

- Big question: is there sufficient s/n to make progress? Not sure.
- Big question: have we really gotten away from center-to-limb systematic errors? Don't know yet.

3. Tim Larson

Medium-l Analysis of Mount Wilson Data

tim larson
tplarson@sun.stanford.edu
Stephen Pinkerton, Ed Rhodes
USC
Jesper Schou
MPS

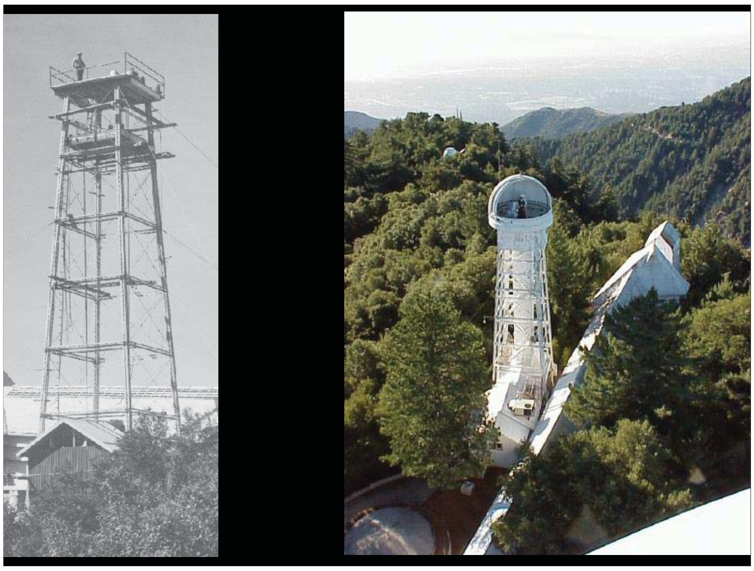

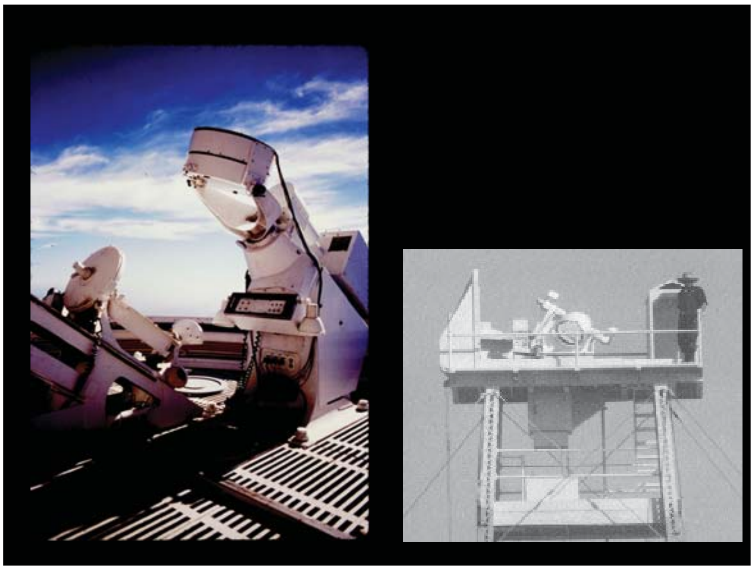

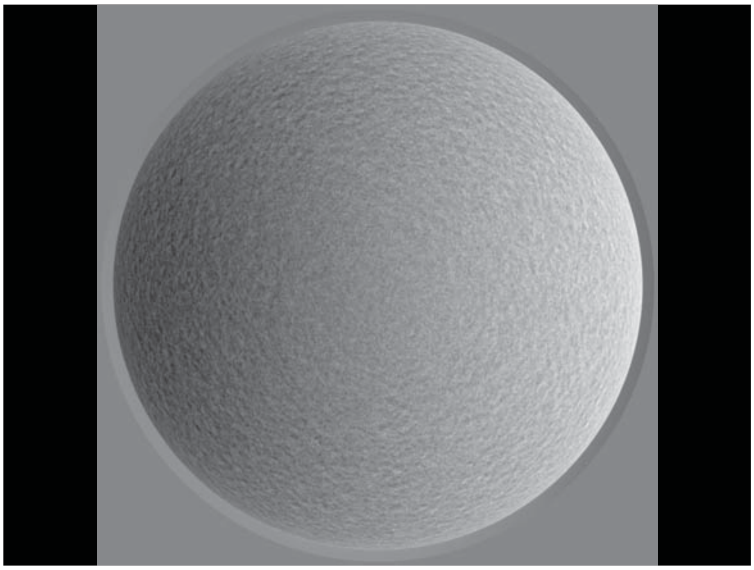

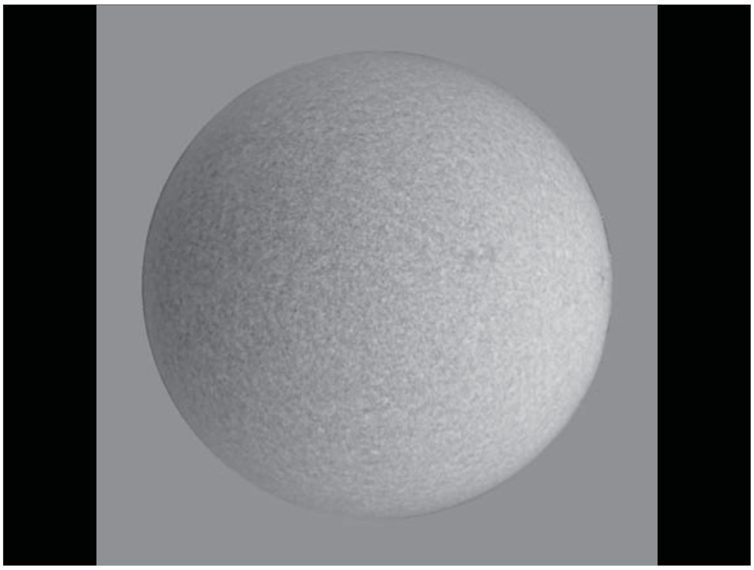

MWO data before MDI

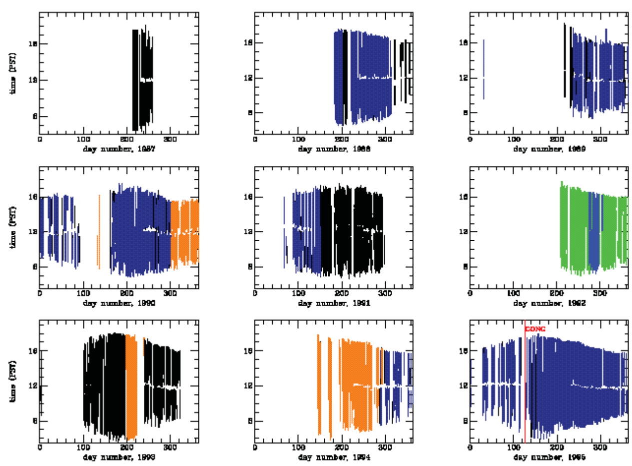

MWO data during MDI

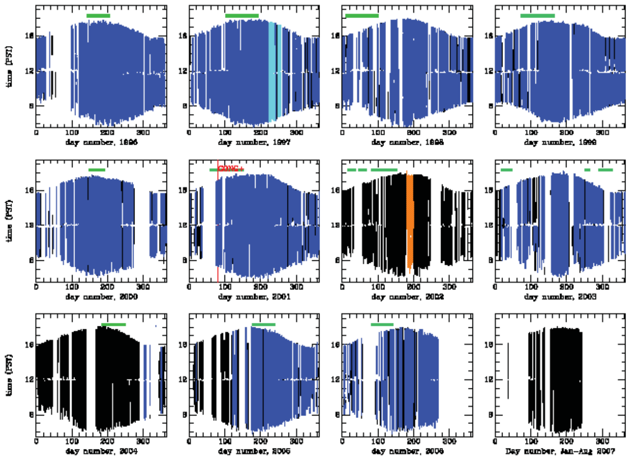

Types of Data

- Filters: Na (mostly) or K (1997)
- Cameras
  - JPL: 1024x1024, 1987-1991
  - PANASONIC: 512x512, 1992-1994, 2007-2009
  - JPL-TALK: 1024x1024, 1994-2007
  - TALKTRONICS: 1024x1024, 2002 (testing)
- Intensity: 1990, 1993-94, 2002

P-angle Drift

- Ring diagram analysis reveals “washing machine” effect
- Auto-correlation with averaged images throughout the day indicates value of 0.018 degrees/hour
- Cross-correlations with MDI indicates value of 0.012 degrees/hour

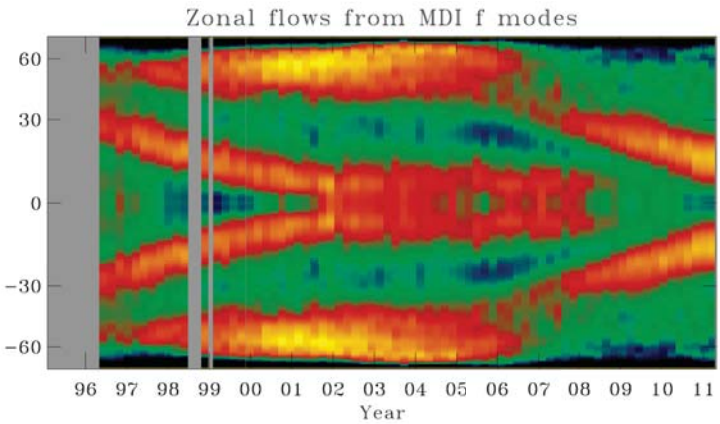

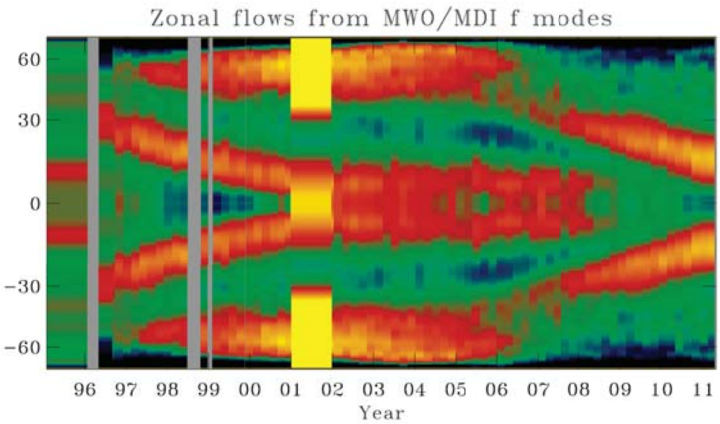

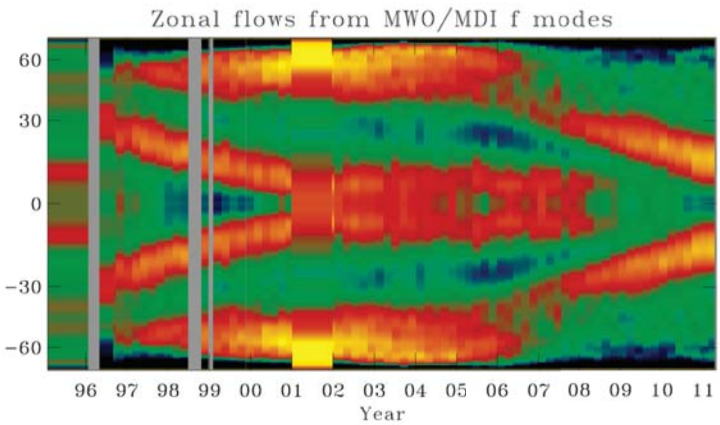

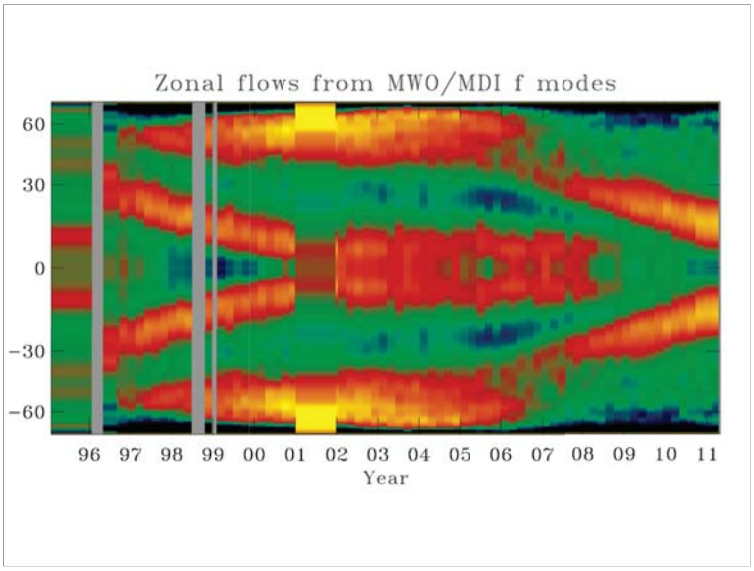

Zonal flows from MWO/MDI f modes
60
30
0
−30
−60
96 97 98 99 00 01 02 03 04 05 06 07 08 09 10 11
Year

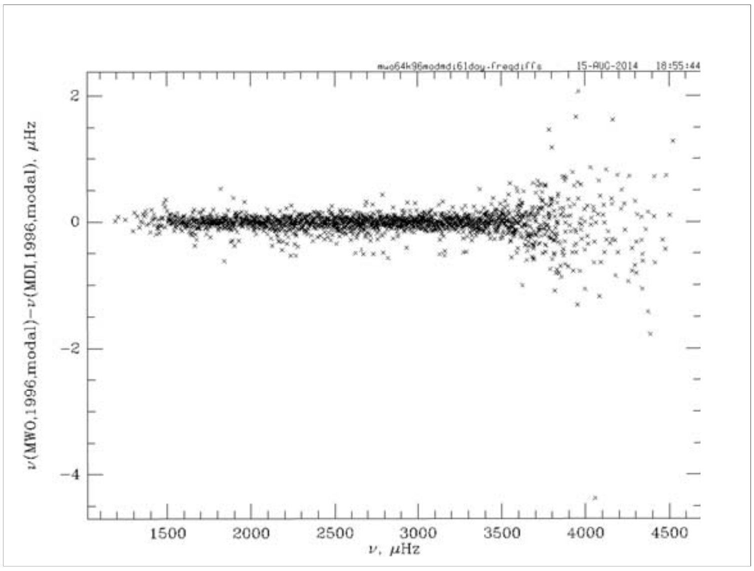

mwo64k96modmdi61day.freqdiffs 15-AUG-2014 18:55:44
2
0
−2
−4
ν(MWO,1996,modal)−ν(MDI,1996,modal), μHz
1500 2000 2500 3000 3500 4000 4500
ν, μHz

That's all Folks!

4. Kaori Nagashima

Nagashima et al. 2014 SoPh

SDO/HMI multi-height velocity measurements

Kaori Nagashima (MPS)

Collaborators:
L. Gizon, A. Birch, B. Löptien, S. Danilovic, R. Cameron (MPS),
S. Couvidat (Stanford Univ.),
B. Fleck (ESA/NASA), R. Stein (Michigan State Univ.)

- *We confirm that we can obtain velocity information from two layers separated by* $\sim {}^{1}/_{2}\, H_\rho$ *from SDO/HMI observations*
- *They are useful for, e.g., multi-layer helioseismology analyses & study of energy transport in the atmosphere, as well as understanding the center-to-limb variations of helioseismology observables?*

2014.09.01.-05.
HELAS VI / SOHO 28 / SPACEINN Helioseismology and Applications@MPS, Göttingen 1

Standard HMI Dopplergram

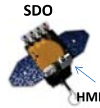

(Couvidat et al. 2012)

- HMI takes filtergrams at 6 wavelengths around Fe I absorption line at 6173 Å
- Calculate the line shift based on the Fourier coefficients of the 6 filtergrams

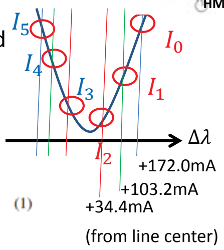

$$a_1 = \frac{2}{T}\int_{-\frac{T}{2}}^{+\frac{T}{2}} I(\lambda)\cos\left(2\pi\frac{\lambda}{T}\right)d\lambda;\qquad b_1 = \frac{2}{T}\int_{-\frac{T}{2}}^{+\frac{T}{2}} I(\lambda)\sin\left(2\pi\frac{\lambda}{T}\right)d\lambda. \qquad (1)$$

$$v = \frac{dv}{d\lambda}\frac{T}{2\pi}\mathrm{atan}\left(\frac{b_1}{a_1}\right)$$

– + some additional calibration to make the standard Dopplergrams (i.e., pipeline products)

Formation layer @ ~100km above the surface (Fleck et al. 2011)
Similar to the formation layer of the center of gravity of the 6 filtergrams. 2

To extract multi-height info, at first, we made 3 simple Dopplergrams. But *it did not work well.*

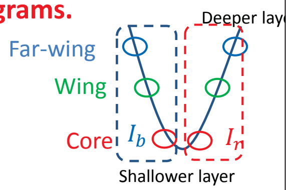

- **Doppler signal:** $\frac{I_b - I_r}{I_b + I_r}$ core, wing, far-wing
- $V = f\left(\frac{I_b - I_r}{I_b + I_r}\right)$
  – fitting the average Doppler signals by 3rd order polynomial using the SDO orbital motion
- wavelength separation (and dynamic range) is limited

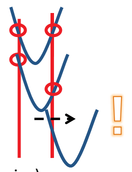

Core is not usable if *v*>1.7km/s

Details: Nagashima et al. 2013 (ASP conference series) 3

We tried several other definitions of Dopplergrams, and found these two look good.

1. Average wing (for deeper layer)
   – Calculate the Doppler signals using the average of each blue and red wing.
   – $\frac{I_b - I_r}{I_b + I_r}$ $\left(I_b = \frac{I_5 + I_4}{2},\ I_r = \frac{I_0 + I_1}{2}\right)$

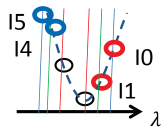

Convert the signal into the velocity:
1. Calculate the average line profile
2. Parallel-Dopplershift the average line profile
3. Calculate the Doppler signals
4. Fit to a polynomial function of the signal

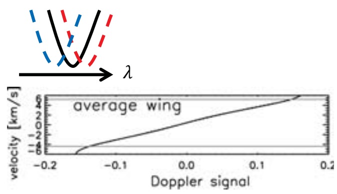

4

We tried several other definitions of Dopplergrams, and found these two look good.

2. Line center (for shallower layer)
   – Doppler velocity of the line center derived from 3 points around the minimum intensity wavelength
   – Calculate the parabola through the 3 points and use its apex as the line shift

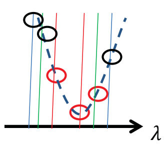

So, we have
1. Average-wing Dopplergrams
2. Line-center Dopplergrams
3. And Standard HMI Dopplergrams (pipeline products)

Now we have 3 Dopplergrams!

Are they really "multi-height"?

5

Are they really "multi-height" Dopplergrams? (1)
→ Estimate of the "formation height" using simulation datasets (STAGGER/MURaM)

6

Are they really "multi-height" Dopplergrams? (1)

⇒Estimate of the "formation height" using simulation datasets

1. Use the realistic convection simulation datasets: STAGGER (e.g., Stein 2012) and MURaM (Vögler et al. 2005)
2. Synthesize the Fe I 6173 Å absorption line profile using SPINOR code (Frutiger et al. 2000)
3. Synthesize the HMI filtergrams using the line profiles, HMI filter profiles, and HMI PSF
4. Calculate three Dopplergrams:
   Line center & Average wing & standard HMI
5. Calculate correlation coefficients between the synthetic Doppler velocities and the velocity in the simulation box

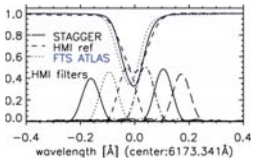

Sample synthetic Dopplergrams (10Mm square)

HMI observation

STAGGER synthetic filtergrams (reduced resolution using HMI PSF, 3.7e2km/pix)

STAGGER synthetic filtergrams (with STAGGER original resolution, 48km/pix)

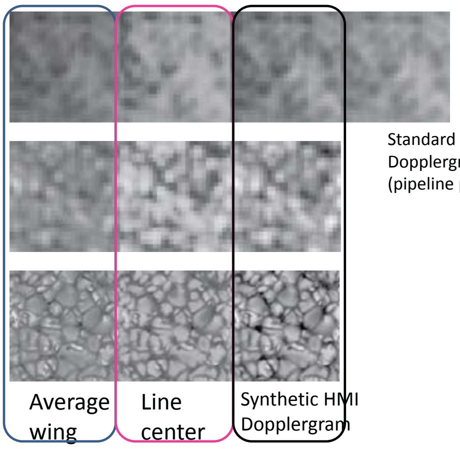

Standard HMI Dopplergram (pipeline product)

Estimate of the "formation height" using simulation datasets

Correlation coefficients between the synthetic Doppler velocities and the velocity in the simulation box

Correlation coefficients

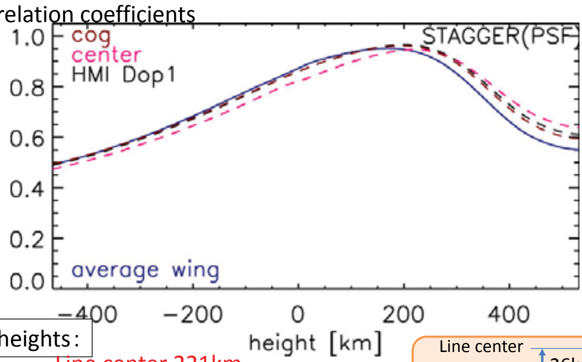

Peak heights:
Line center 221km
Standard HMI 195 km
Average wing 170 km

Line center – Standard HMI: 26km
Standard HMI – Average wing: 25km

Estimate of the "formation height" using simulation datasets

Correlation coefficients between the synthetic Doppler velocities and the velocity in the simulation box

Correlation coefficients **(with original STAGGER resolution (no HMI PSF))**

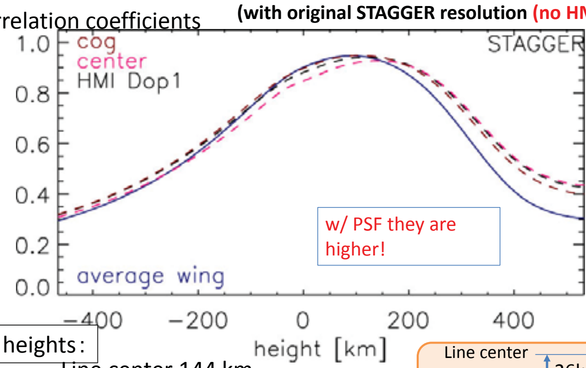

w/ PSF they are higher!

Peak heights:
Line center 144 km
Standard HMI 118km
Average wing 92km

Line center – Standard HMI: 26km
Standard HMI – Average wing: 25km

Estimate of the "formation height" using simulation datasets

Correlation coefficients between the synthetic Doppler velocities and the velocity in the simulation box

Correlation coefficients **MURaM simulation data** 17.6km/pix

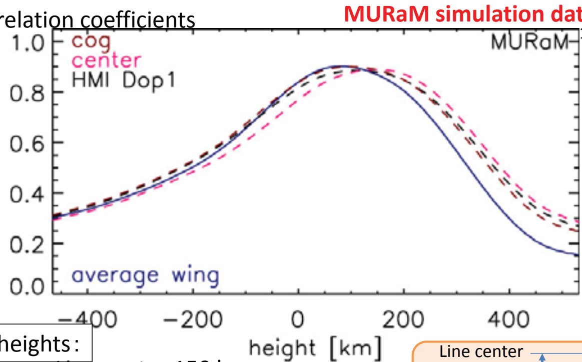

Peak heights:
Line center 150 km
Standard HMI 110 km
Average wing 80 km

Line center – Standard HMI: 40km
Standard HMI – Average wing: 30km

The correlation coefficients has a wide peak

← *Vz* itself has a wide correlation peak

Vz auto-correlation coefficient in the wavefield

STAGGER (original resolution)

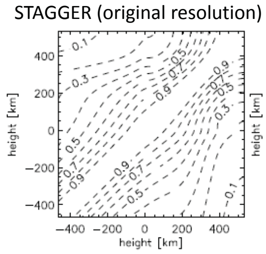

STAGGER (w/ HMI PSF)

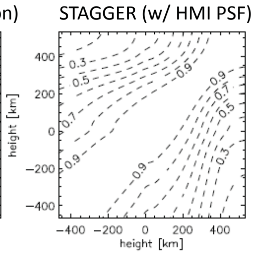

The width of the correlation peak is so large.

Therefore, the Dopplergram of this wavefield should have such a wide range of contribution heights.

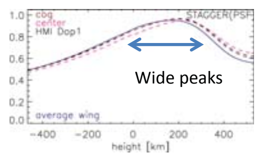

Contribution layer is higher when the resolution is low (i.e.,w/ PSF)

- *If the formation height in the cell is higher*
  - In the cell it is brighter than on the intergranular lane
  - The cell contribution is larger than the intergranular lane's contribution?
  - Therefore, the contribution layer is higher?

STAGGER simulation data

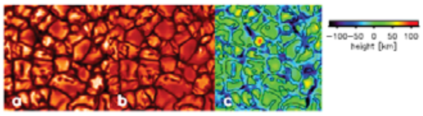

a) Continuum intensity map b) Surface vertical velocity map c) $\tau = 1$ layer height map

Are they really "multi-height" Dopplergrams? (2)
→ Phase difference measurements

Phase difference between Doppler velocity datasets from two different height origins

Line center
HMI a
b
Average wing

HMI observation data

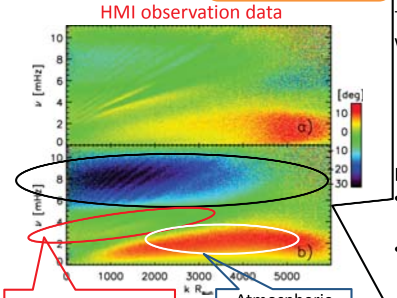

The waves above the photospheric acoustic cutoff (~5.4mHz) can propagate upward.

-> Phase difference between two layers with separation Δz : $\frac{\Delta\phi}{2\pi\nu} = \frac{-\Delta z}{c_s}$

Significant phase difference is seen. Surely they are from different height origin.

Rough estimate:

- Photospheric sound speed: $c_s \sim 7$ km/s
- Phase difference measured: $\Delta\phi = -30[\text{deg}]@8\text{mHz}$

- $\Rightarrow \Delta z \sim 73\text{km}$

This means...what?

No significant phase difference (in p-mode regime)

Atmospheric gravity wave ? (e.g., Straus et al. 2008, 2009)

Check the height difference with Response function

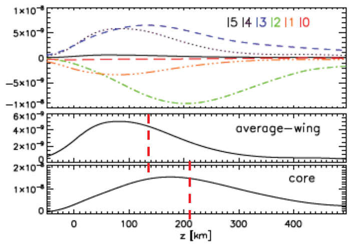

Center of gravity of R_{br}

Average-wing: 140km

Core : 210km

Difference 70km

Height dif. Estimated using the phase dif. (shown in the previous page) $\Delta z \sim 73$km

We calculate Response function using STOPRO in SPINOR code (Frutiger et al. 2000)

Definition:

$\mathrm{I}(\lambda, v'_z) - \mathrm{I}(\lambda, v_z)$

$= I_{cont} \int d\tau R(\tau, \lambda, v_z)[v'_z(\tau) - v_z(\tau)]$

$v_z(\tau)$: vertical velocity field at optical depth τ

* Calculate at each pixel, and average over an area with 10Mm square.

For simplicity,

Simple Doppler signal:

$$D_{br} = \frac{I(\lambda_b) - I(\lambda_r)}{I(\lambda_b) + I(\lambda_r)}$$

If we assume the denominator of D_{br} does not have much dependence on the velocity,

$R_{br} \sim R_b - R_r$

Phase difference
Observed data VS Simulated data (STAGGER)

Cadence 45sec

Cadence 60sec

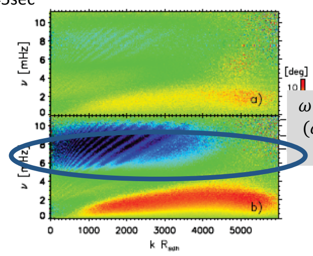

$\omega > \omega_{cut}$ similar (ω_{cut} is lower in STAGGER)

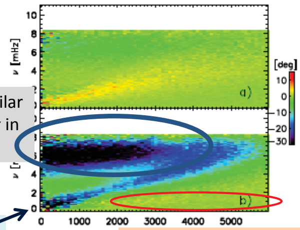

Ridge?

Line center
HMI a
b
Average wing

Very weak atmospheric gravity wave feature

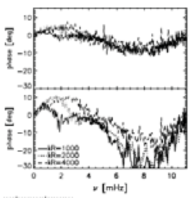

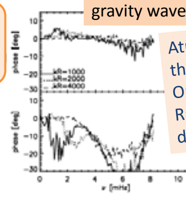

Atmosphere is thin? (~550km) Or difference in Radiative damping?

Phase difference (CO^5BOLD case)

Fig. 1 in Straus et al. 2008

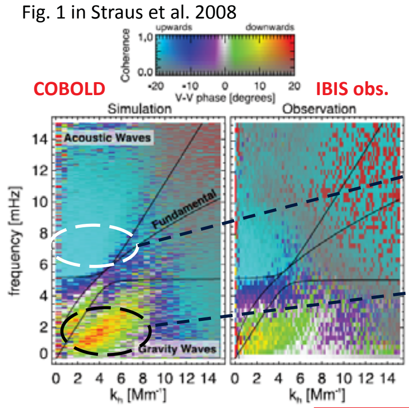

Phase difference of the velocity fields at 250km and 70km above surface

They have

-negative phase shift above the acoustic cutoff

Same as STAGGER's results

Positive phase shift in the lower frequency ranges (atmospheric gravity waves)

Different from STAGGER's results

Upper boundary of the atmosphere: STAGGER 550km, CO^5BOLD 900km

Power map of HMI-algorithm Dopplergram

HMI observation   STAGGER

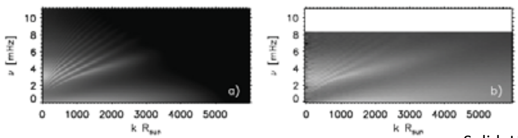

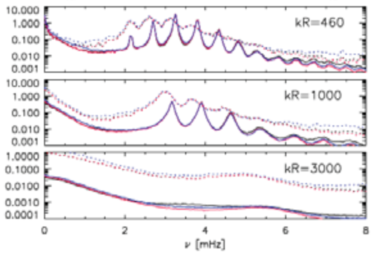

Solid: HMI obs.
Dotted: STAGGER

- Line-center
- HMI-algorithm
- Average-wing

In the STAGGER power map there are some power enhance in the convection regime.

So… summary of the phase difference

- P-mode regime: phase difference is small because they are eigenmonds.
- $\omega > \omega_{\text{cut}}$: upward-propagating wave
  - phase difference found in observation data and STAGGER data have similar trends.
  - ω_{cut} in STAGGER atmosphere is *lower* than that of the Sun.
- Convective regime (lower frequency, larger wavenumber)
  - Observation: positive phase difference indicates the atmospheric gravity waves
  - STAGGER : no such feature
    - Atmospheric extent (about 550km) of STAGGER data might not be sufficient for the atmospheric gravity waves?
    - Radiative damping of the short-wavelength waves in the STAGGER is stronger than the Sun?
    - or…?

Summary

- We propose two Dopplergrams other than the standard HMI-algorithm Dopplergram:
  - line-center Dopplergram (30-40 km above the standard)
  - Average-wing Dopplergram (30-40 km below the standard)
- These are useful for understanding the center-to-limb variation of helioseismology observables (e.g., Zhao et al. 2012) ?

Center-to-limb variation of $\tau = 1$ layer height at 5000Å (continuum)
Calculation was done by SPINOR code

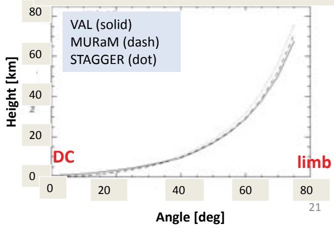

The formation layer heights is higher in the region nearer the limb.

5. Vincent Böning

Extension to Spherical Geometry - Sensitivity Kernels for Flows in Time-Distance Helioseismology

Vincent Böning

Kiepeneuer-Institut für Sonnenphysik, Freiburg

04.09.2014

Collaborators:
M. Roth & W. Zima, KIS Freiburg

contact: vboening@kis.uni-freiburg.de

Kiepenheuer-Institut für Sonnenphysik

UNI FREIBURG

erc European Research Council
Established by the European Commission

Motivation: We need spherical Kernels.

- They are already used in the current scientific debate, e.g. :
  - Meridional flow measurements: e.g. Zhao et al. (2013), Kholikov et al. (2014).
  - Studies on supergranules: e.g. Duvall & Hanasoge (2013), Duvall et al. (2014).
  - → Both perform modelling with ray approximation kernels.
- Born kernels not yet available in spherical geometry.
- Cartesian Born kernels used in HMI pipeline for subsurface flow inversions (e.g. Zhao et al., 2012).

Graphics: R. Arlt, AIP

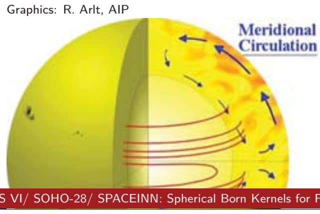

How to calculate Born Kernels?

- Using general recipe of Gizon and Birch (2002), and for flows Birch and Gizon (2007) = BG2007.
  - Solve zero and first order damped and stochastically driven wave equation.
  - Via Green's functions, using Model S eigenfunctions.
  - Find expression for perturbed cross-correlation.
  - Find travel-time difference shift as a function of flow: $\delta\tau_{\text{diff}} = \int \mathbf{K} \cdot \mathbf{v} \, \mathrm{d}^3 r$.

How to calculate Born Kernels?

- Using general recipe of Gizon and Birch (2002), and for flows Birch and Gizon (2007) = BG2007.
  - Solve zero and first order damped and stochastically driven wave equation.
  - Via Green's functions, using Model S eigenfunctions.
  - Find expression for perturbed cross-correlation.
  - Find travel-time difference shift as a function of flow: $\delta\tau_{\text{diff}} = \int \mathbf{K} \cdot \mathbf{v} \, \mathrm{d}^3 r$.

→ And how to do spherical?

How to calculate Born Kernels?

- Using general recipe of Gizon and Birch (2002), and for flows Birch and Gizon (2007) = BG2007.
  - Solve zero and first order damped and stochastically driven wave equation.
  - Via Green's functions, using Model S eigenfunctions.
  - Find expression for perturbed cross-correlation.
  - Find travel-time difference shift as a function of flow: $\delta\tau_{\text{diff}} = \int \mathbf{K} \cdot \mathbf{v} \, \mathrm{d}^3 r$.

→ And how to do spherical?
  - First attempts by Roth, Gizon & Birch (2006).
  - Expand Green's functions in spherical harmonics.
  - Find a formula that can actually be calculated numerically.
  - Validate the method.

Sanity Check: The Cartesian Limit

Sanity Check: The Cartesian Limit

- With A. C. Birch & L. Gizon.
- Setup: point-to-point travel-times on equator, $\Delta = 10\,\mathrm{Mm}$
- $K_\phi(r,\theta,\phi) = K_x(x,y,z)$, sensitivity for zonal flows, horizontal cuts.
- Line asymmetry not taken into account: Both results only using f-mode ridge in computation.

Spherical:

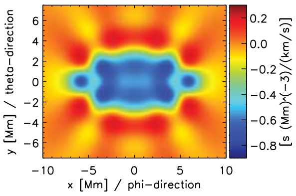

Cartesian (BG2007 code):

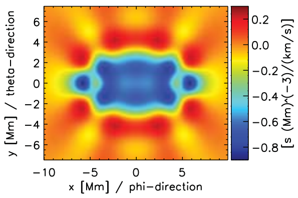

Maximum value: 8 % off.

Sanity Check: The Cartesian Limit

Horizontal integrals: $K_\phi = K_x$, sensitivity for zonal flows.

From Cartesian BG2007 code (solid) and from spherical code (dashed).

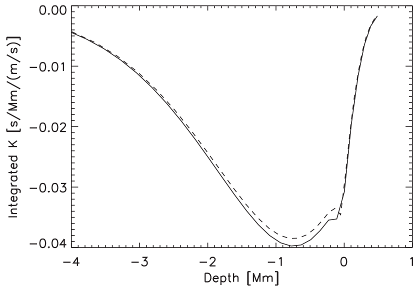

Maximum value: 3 % off. Similar to additional consistency tests.

Validation of Method with Simulated Data

- Data and flow model (right) from Hartlep et al. (2013).
- Original flow model from Rempel (2006), amplified by factor of 36: $v_{\mathrm{max}} = 500\,\mathrm{m/s}$ at the surface.
- → Do simulated and forward-modelled travel-times agree?
- Analysis done without filters, proceeding similarly to Hartlep et al. (2013).

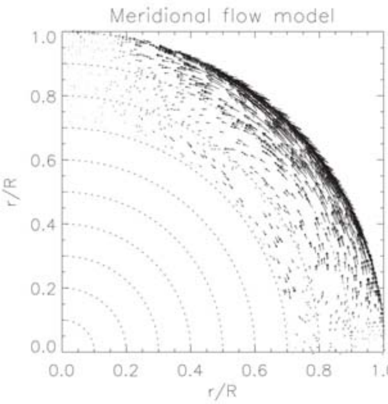

Validation of Method with Simulated Data

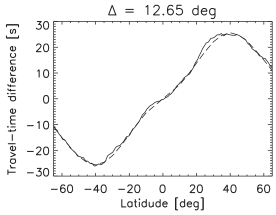

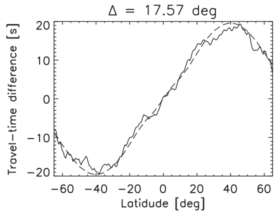

- Travel-times fitted with Gizon and Birch (2004) procedure to simulated data (solid line).
- Travel-times from forward-model, i.e. kernel integrated over flow model (dashed line).
- Travel-time differences: S-N!

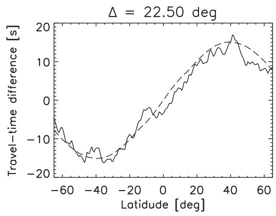

Deep Meridional Flow Kernels: First results

- We compare kernels with different filters (no filter, low-pass in l, phase-speed).
- K_θ, i.e. sensitivity to southward flow,
- cuts at central meridian and just below photosphere,
- $\Delta = 42.19\,\mathrm{deg}$ in N-S-direction,
- centered at latitude 40 degrees north,
- computation uses $l \leq 170$, same as simulation in Hartlep et al. (2013),
- modelling radial component of wavefield.

Unfiltered, $\Delta = 42.19\,\mathrm{deg}$

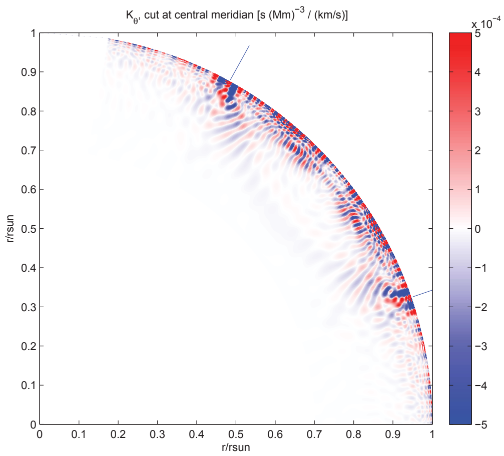

Unfiltered, $\Delta = 42.19\,\mathrm{deg}$

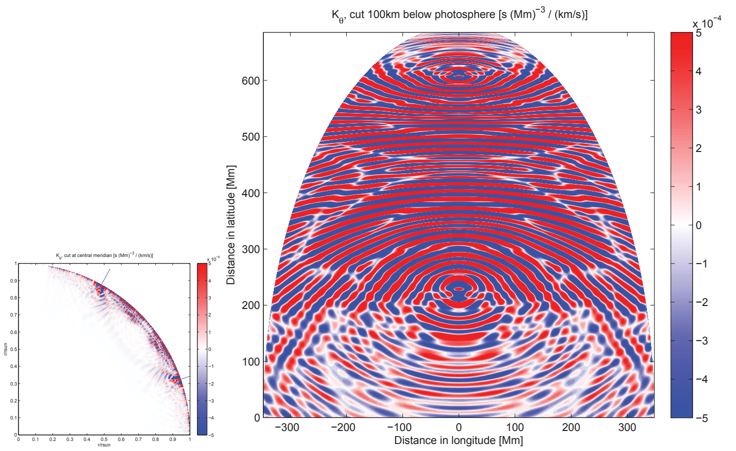

Unfiltered, $\Delta = 42.19\,\mathrm{deg}$

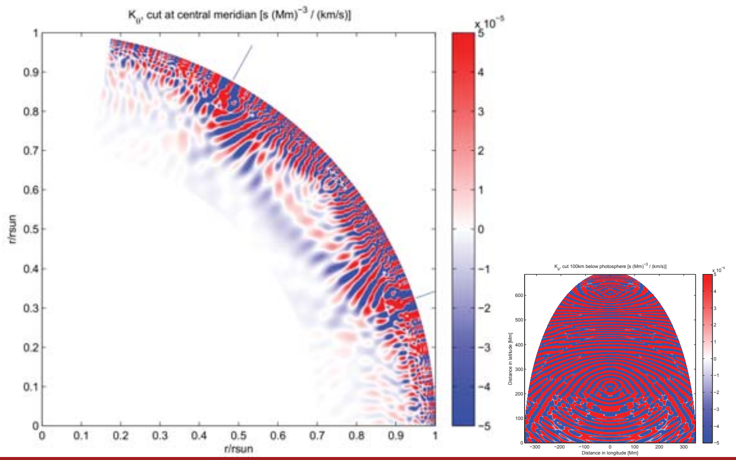

$\Delta = 42.19\,\mathrm{deg}$, filtered: $F(l,\omega) = \exp(-\frac{l^2}{2\,\delta l^2})$, $\delta l = 50$

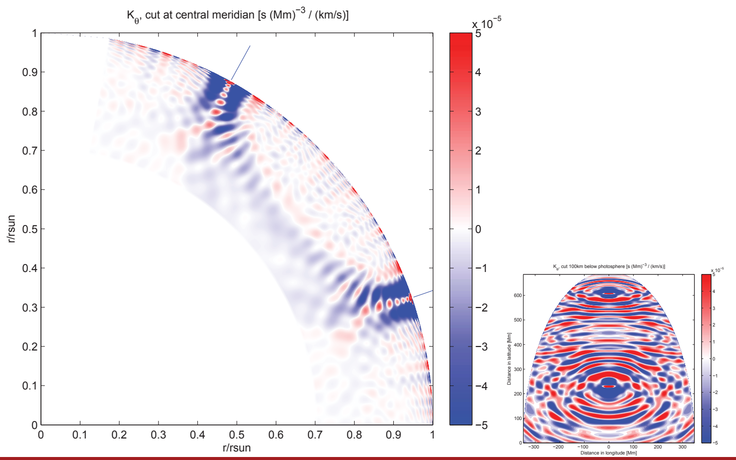

$\Delta = 42.19\,\mathrm{deg}$, filtered: $F(l,\omega) = \exp(-\frac{l^2}{2\,\delta l^2})$, $\delta l = 20$

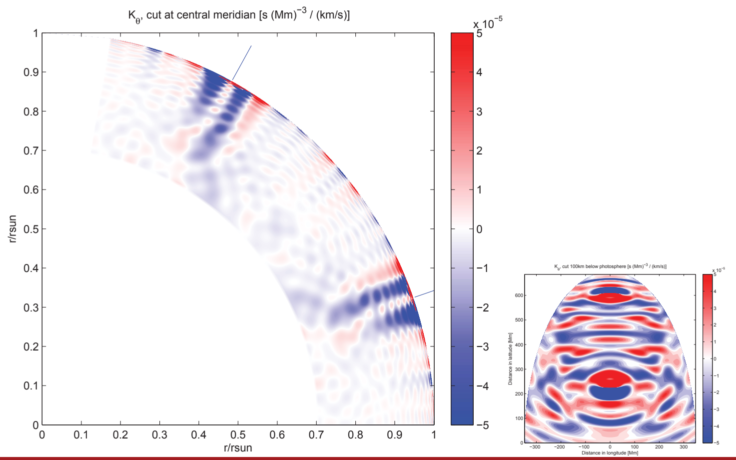

Phase-speed filt., $v_0 = 284.3\,\mathrm{km/s}$, $\delta v = 7\,\mathrm{km/s}$ (Kholikov et al., 2014)

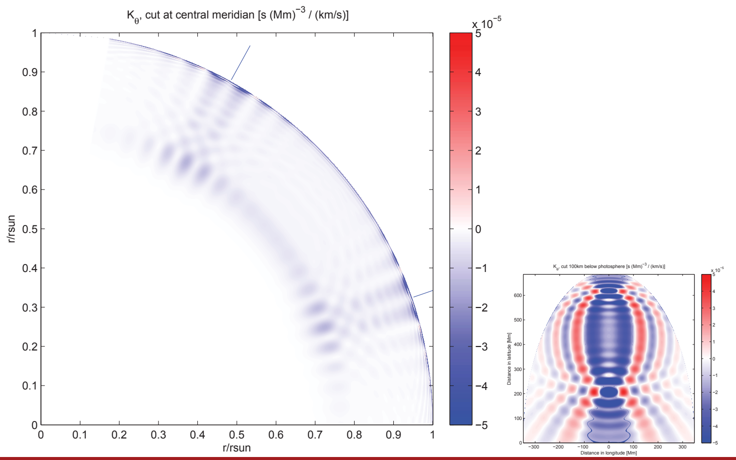

Phase-speed filt., $v_0 = 284.3\,\mathrm{km/s}$, $\delta v = 7\,\mathrm{km/s}$, $\Delta = 42.19\,\mathrm{deg}$

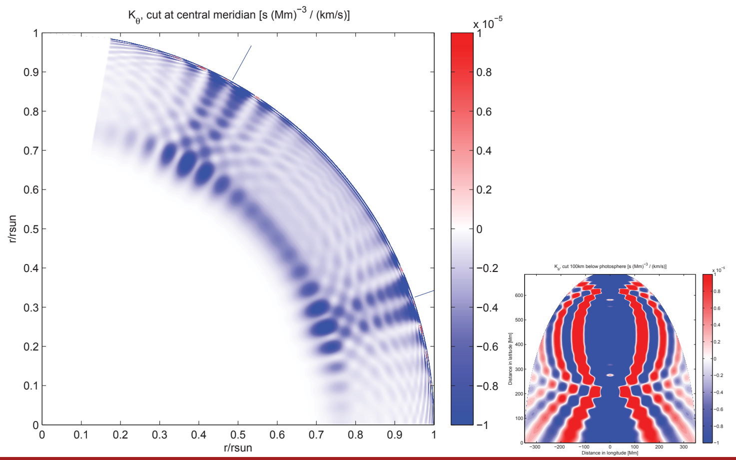

How big is the sensitivity to the return flow? ($\Delta = 42\,\mathrm{deg}$)

- Kernel integrated over Hartlep et al. (2013) meridional flow profile.

Kernel	$\delta\tau$ for $r/R_\odot \leq 0.79$	% of total $\delta\tau$	ray kernels *
unfiltered	-0.446 s	10.4 %	$\approx$ 20 %
$\delta l = 50$	-0.489 s	13.4 %	
$\delta l = 20$	-0.467 s	14.8 %	
phase-sp.	-0.503 s	11.4 %	

Table: * Ray kernel value from Hartlep et al. (2013).

How big is the sensitivity to the return flow? ($\Delta = 42\,\mathrm{deg}$)

- Kernel integrated over Hartlep et al. (2013) meridional flow profile.

Kernel	$\delta\tau$ for $r/R_\odot \leq 0.79$	% of total $\delta\tau$	ray kernels *
unfiltered	-0.446 s	10.4 %	$\approx$ 20 %
$\delta l = 50$	-0.489 s	13.4 %	
$\delta l = 20$	-0.467 s	14.8 %	
phase-sp.	-0.503 s	11.4 %	

Table: * Ray kernel value from Hartlep et al. (2013).

- Divide $\delta\tau$ by ≈ 25 to get realistic numbers: $\delta\tau_{\leq 0.79} \approx 0.02\,\mathrm{s}$!
- The sensitivity is always concentrated in the upper convection zone.
- Ray and Born kernel values are quite different. Is that a problem?

How big is the sensitivity to the return flow? ($\Delta = 42\,\mathrm{deg}$)

- Kernel integrated over Hartlep et al. (2013) meridional flow profile.

Kernel	$\delta\tau$ for $r/R_\odot \leq 0.79$	% of total $\delta\tau$	ray kernels *
unfiltered	-0.446 s	10.4 %	$\approx$ 20 %
$\delta l = 50$	-0.489 s	13.4 %	
$\delta l = 20$	-0.467 s	14.8 %	
phase-sp.	-0.503 s	11.4 %	

Table: * Ray kernel value from Hartlep et al. (2013).

- Divide $\delta\tau$ by ≈ 25 to get realistic numbers: $\delta\tau_{\leq 0.79} \approx 0.02\,\mathrm{s}$!
- The sensitivity is always concentrated in the upper convection zone.
- Ray and Born kernel values are quite different. Is that a problem?

⇒ Unfiltered kernel has smallest sensitivity to return flow.
⇒ Low-pass filtering in l gives the strongest relative sensitivity to return flow.
⇒ Phase-speed filtered kernels are best localised at the target depth.

Summary

1. We can adequately calculate spherical Born kernels:
   - ✓ Results from Cartesian geometry (BG2007) reproduced.
   - ✓ Effect of meridional flow correctly modelled (Hartlep et al., 2013).

Summary

1. We can adequately calculate spherical Born kernels:
   - ✓ Results from Cartesian geometry (BG2007) reproduced.
   - ✓ Effect of meridional flow correctly modelled (Hartlep et al., 2013).
2. Example kernels for meridional flow measurements:
   - 10-15% of the total sensitivity is due to the return flow for a standard meridional flow profile.
   - Ray and Born kernels have different sensitivity to return flow by a factor of 2.
   - Low-pass filtering in l gives the strongest relative sensitivity to return flow.
   - Phase-speed filtered kernels are best localised at target depth.

Summary

1. We can adequately calculate spherical Born kernels:
   - ✓ Results from Cartesian geometry (BG2007) reproduced.
   - ✓ Effect of meridional flow correctly modelled (Hartlep et al., 2013).
2. Example kernels for meridional flow measurements:
   - 10-15% of the total sensitivity is due to the return flow for a standard meridional flow profile.
   - Ray and Born kernels have different sensitivity to return flow by a factor of 2.
   - Low-pass filtering in l gives the strongest relative sensitivity to return flow.
   - Phase-speed filtered kernels are best localised at target depth.

Thank you very much!

References

- Zhao et al. (2013)
- Kholikov et al. (2014)
- Duvall & Hanasoge (2013)
- Duvall et al. (2014).
- Zhao et al. (2012)
- Gizon and Birch (2002)
- Birch and Gizon (2007, BG2007)
- Roth, Gizon & Birch (2006)
- Hartlep et al. (2013)
- Rempel (2006)
- Gizon and Birch (2004)

Power: kernel vs simulated data

Unfiltered power integrated over k, normalized, for Hartlep et al. 2013 (solid) and spherical kernels (dashed), using $l \leq 169$:

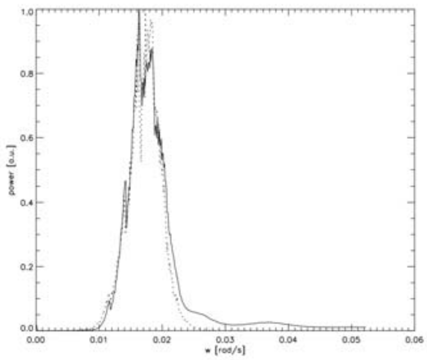

Unfiltered Kernel

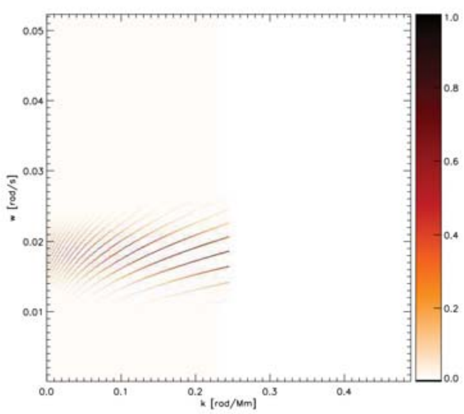

Low-pass l, $\delta l = 50$

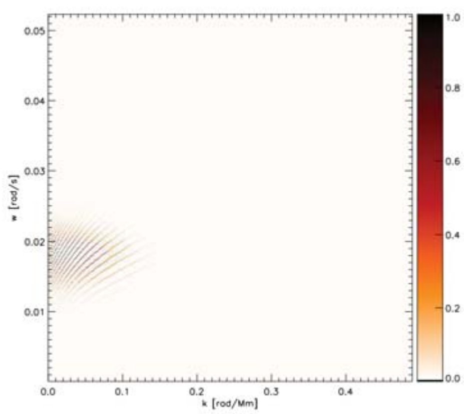

Low-pass l, $\delta l = 20$

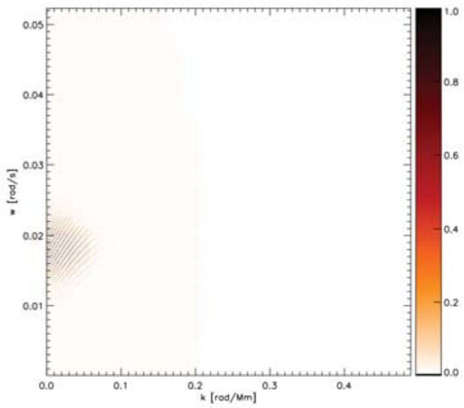

Phase-speed

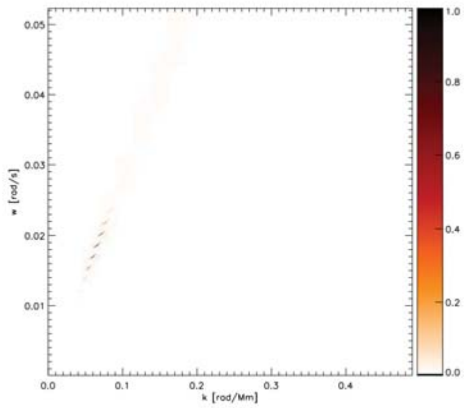

Unfiltered Kernel

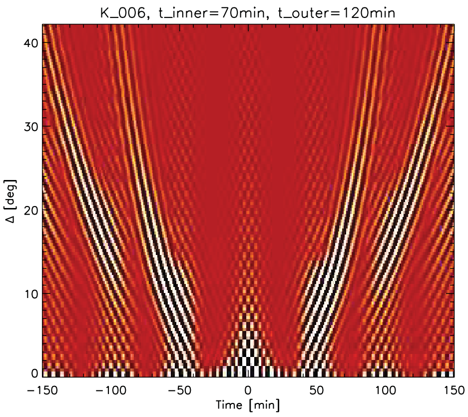

Low-pass l, $\delta l = 50$

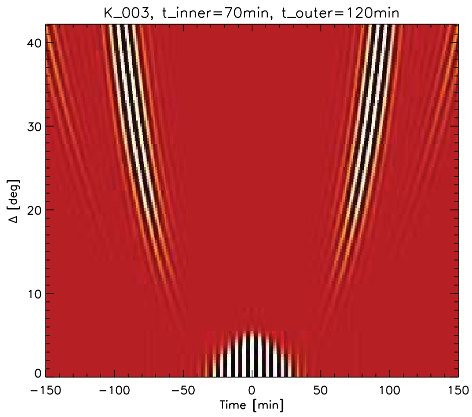

Low-pass l, $\delta l = 20$

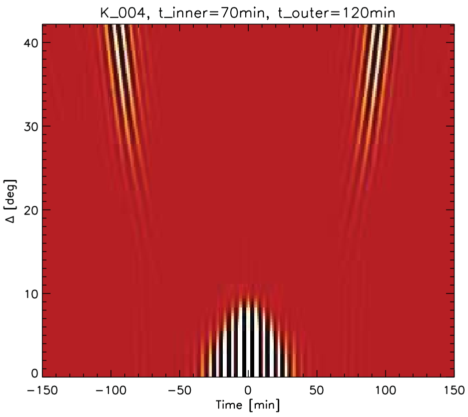

Phase-speed

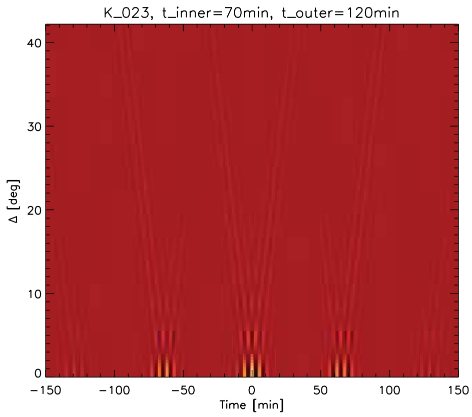

$v_{\max} = 500\,\text{m/s}$ still in linear regime?

For $\Delta = 22.5\,\text{deg}$, travel-times from E-W-kernel (dashed) at equator and *exact* perturbed cross-correlation (crosses, method see Jackiewicz et al., 2007) for a solid body rotation corresponding to a certain equatorial zonal flow speed (x-axis): Linear regime extends to these flow speeds.

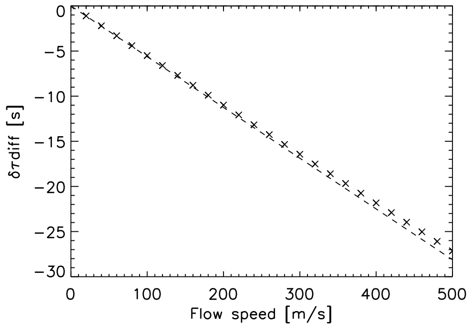

Sanity Check: The Cartesian Limit

$K_\phi = K_x$, sensitivity for zonal flows, integrated wrt depth, cut along $y = 0$:

Spherical:

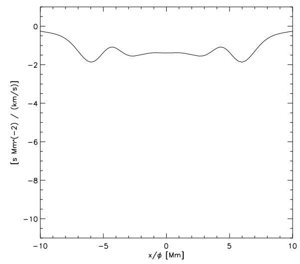

BG2007-Code (Cartesian)

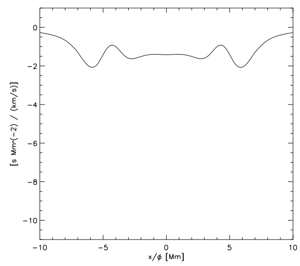

Sanity Check: The Cartesian Limit

$K_\phi = K_x$, sensitivity for zonal flows.

Spherical:

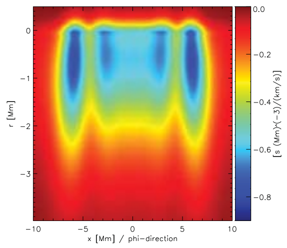

BG2007-Code (Cartesian)

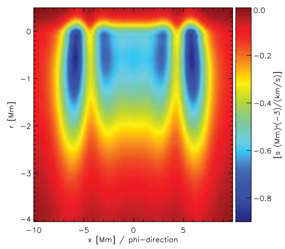

Maximum value: 8 % off.

Sanity Check: The Cartesian Limit

$K_\theta = -K_y$, sensitivity for meridional flows.

Spherical:

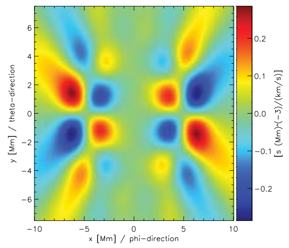

BG2007-Code (Cartesian)

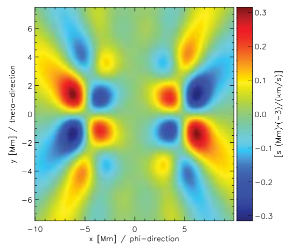

Sanity Check: The Cartesian Limit

$K_r = K_z$, sensitivity for convective flows.

Spherical:

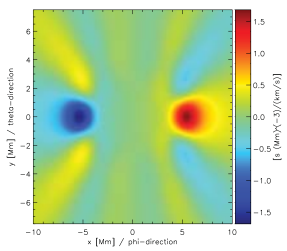

BG2007-Code (Cartesian)

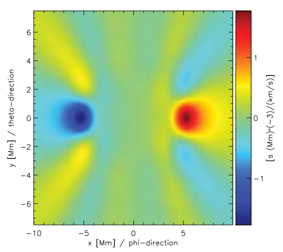

6. Ariane Schad

European Research Council

fdm

KIS Kiepenheuer-Institut für Sonnenphysik

Distortion of global mode eigenfunctions - Measuring meridional flow and solar rotation

Ariane Schad[1,2], Jens Timmer[2], Markus Roth[1]

[1]Kiepenheuer-Institut für Sonnenphysik

[2]Freiburg Center for Data Analysis and Modeling, University of Freiburg

HELAS VI / SOHO-28 / SpaceInn

04 September 2014

Göttingen, Germany

Perturbation & coupling of p-modes

> flows lead to a coupling of modes in a „neighborhood" K_k of a mode k=(n,l,m):

$$\boldsymbol{\xi}_k(r,\theta,\phi) = \sum_{k' \in K_k} c_{kk'} \boldsymbol{\xi}^0_{k'}(r,\theta,\phi)\,,$$

(Lavely & Ritzwoller 1992)

perturbed eigenfunction — unperturbed eigenfunction

> $c_{kk'}$ – coupling coefficient between mode k,k' (≈coupling strength):

$$c_{kk'} \approx -2\,\mathrm{i}\,\frac{\omega_k}{\omega_k^2 - \omega_{k'}^2} \int \rho_0\, \overline{\boldsymbol{\xi}^0_{k'}} \cdot \underbrace{(\boldsymbol{u} \cdot \nabla \boldsymbol{\xi}^0_k)}_{\text{advection of acoustic wave}}\, d^3\boldsymbol{r} \in \mathbb{C}\,, \quad k' \in K_k$$

(1. order approximation)

(Schad et al., ApJ, 2011)

Perturbation & coupling of p-modes due to meridional flow

Spherical harmonic representation of **u**:

$$\boldsymbol{u}(\boldsymbol{r}) = \sum_{s=1}^{\infty} [\underbrace{u_s^0(r) Y_s^0(\theta,\phi)\boldsymbol{e}_r}_{\text{radial component}} + \underbrace{v_s^0(r)\partial_\theta Y_s^0(\theta,\phi)\boldsymbol{e}_\theta}_{\text{horizontal component}}]$$

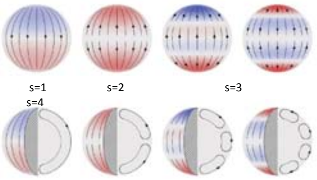

(Figure source: D. Hathaway, NASA)

conservation of mass: $\rho_0 r s(s+1) v_s^0 = \partial_r (r^2 \rho_0 u_s^0)$

Polynomial expansion of coupling coefficients:

$$c_{kk'} = c_{kk'}(m) \approx \mathrm{i}\,\frac{\omega_k}{\omega_k^2 - \omega_{k'}^2} \sum_s b^s_{k'k} \mathcal{P}^s_{k'k}(m)$$

b-coefficients: $b^s_{k'k} = \int_0^R \rho_0(r) K_s^{k'k}(r) u_s^0(r) r^2 dr$

(Schad et al., ApJ, 2011)

> knowing $\{b^s_{k'k}\}$ one can infer the flow coefficients $u_s(r)$ & $v_s(r)$!

Effect of mode coupling on global oscillation data

SHT of full-disk Dopplergrams:

$$o_{l'm'}(t) = \int \overline{Y^{m'}_{l'}}(\theta,\phi) W(\theta,\phi) v_D(\theta,\phi,t) d\Omega = \sum_k \alpha_k(t) \sum_{k'' \in K_k} c_{kk''} \xi^r_{k''}(R) L_{k'k''}$$

$L_{k'k''}$ - leakage matrix elements (imperfect orthogonality: line of sight projection, solar disk, etc.)

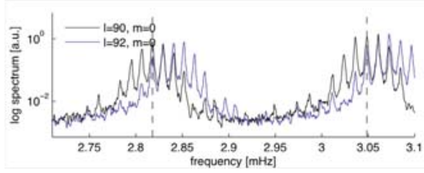

Measure for cross-talk in SHT data: (Fourier) amplitude ratio: between reference mode k=(n,l,m) and coupling modes k'

$$y_{kk'}(\omega_k) = \frac{\tilde{o}_{l'm'}(\omega_k)}{\tilde{o}_{lm}(\omega_k)} \approx \frac{\sum_{k''} c_{kk''} \xi^r_{k''}(R) L_{k'k''}}{\sum_{k''} c_{kk''} \xi^r_{k''}(R) L_{kk''}} \in \mathbb{C} \qquad \langle y_{lm,l'm}(\omega_{nlm}) \rangle = \frac{C S_{lm,l'm}(\omega_{nlm})}{S_{lm}(\omega_{nlm})},$$

(Schad et al., ApJ, 2011)

(Schad et al., ApJL, 2013)

Application to MDI data - superimposed flow components (s =2,4,6,8)

> MDI data 2004-2010, 1 ≤ l ≤ 200, s=1,...,8

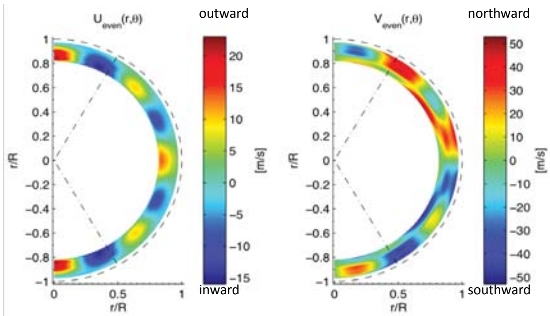

(Schad et al., ApJL 2013)

> complex flow pattern in latitude & depth

> in contrast to „prevalent" picture of two flow cells

Evaluation of the method

How can we evaluate the method and the reliability of the result?

> analysis of simulated acoustic wave fields

> comparison of flow measurements from different methods: here for rotation!

Evaluation: Analysis of simulated acoustic wavefield

-3D simulation of acoustic wavefield (T. Hartlep et al. 2013)
- meridional flow (500 m/s)
- T ≈ 2.7d
- dt = 30s
- l = 1,...,170
- without leakage

simulated flow

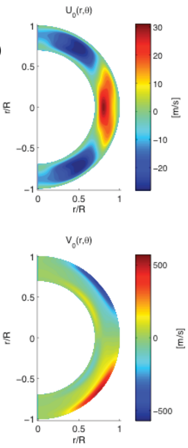

Evaluation: Analysis of simulated acoustic wavefield - results

-3D simulation of acoustic wavefield (T. Hartlep et al. 2013)
- meridional flow (500 m/s)
- T ≈ 2.7d
- dt = 30s
- l = 1,...,170
- without leakage

> s = 2,...,8
> inversion results resembles flow model
> deviations near surface & base of CZ (l<=170, short T)

simulated flow

inversion result

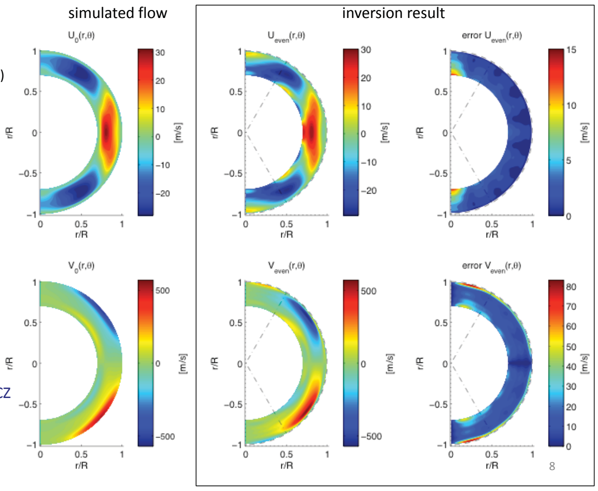

Evaluation: Mode coupling due to rotation - extension

Toroidal velocity field of solar rotation:

$$\boldsymbol{u}_{rot}(r,\theta,\phi) = \Omega(r,\theta) r \sin\theta\, \boldsymbol{e}_\phi = -\sum_s w_s(r)\partial_\theta Y_s^0(\theta,\phi)\boldsymbol{e}_\phi$$

(Ritzwoller & Lavely 1991)

s = num. of zonal bands in latitude

Extension of coupling coefficient:

$$c_{kk'} = c_{kk'}^{(rot)} + c_{kk'}^{(merid.)} \approx \frac{\omega_k}{\omega_k^2 - \omega_{k'}^2}\sum_s (a_{k'k}^s + \mathrm{i}\, b_{k'k}^s)\mathcal{P}_{k'k}^s(m)$$

(Schad, Dissertation 2013, Vorontsov MNRAS 2011)

Expansion coefficients: $$a_{k'k}^s = \int_0^R \rho_0(r) T_s^{k'k}(r)\, w_s^0(r)\, r^2 dr$$

$$b_{k'k}^s = \int_0^R \rho_0(r) K_s^{k'k}(r) u_s^0(r) r^2 dr$$

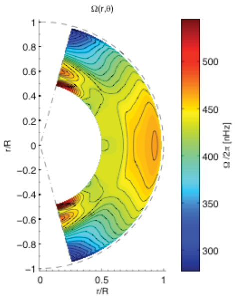

Influence of rotation on amplitude ratios

Amplitude ratios from MDI data vs. flow model (coupling modes: n=1, l=180 and n'=1, l'=182):

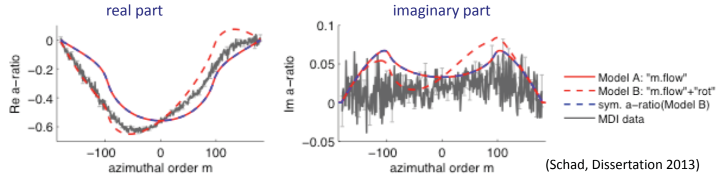

(Schad, Dissertation 2013)

> azimuthal asymmetry

> can be explained by the influence of rotation

> symmetrization of a-ratios in „m“ can compensate for rotation effect

Inversion for rotation – first results

$$\Omega(r,\theta) r \sin\theta = -\sum_s w_s(r)\partial_\theta Y_s^0(\theta,\phi)$$

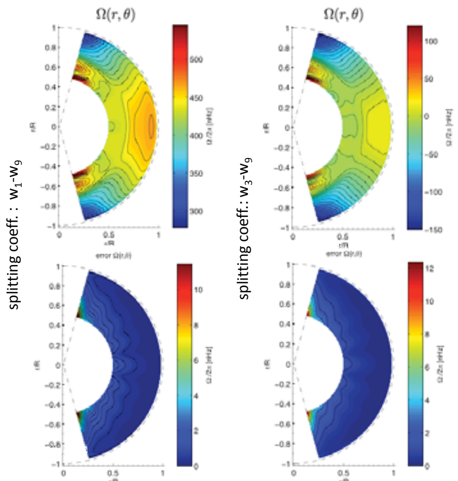

> Rotationrate profile from splitting - coefficients (J. Schou)

$$\omega_{nlm} = \omega_{nl0} + \sum_s \alpha_{nl}^s P_{sl}(m)$$

- MDI data (2004-2010)

- 1 ≤ l ≤ 200

- superimpose components with s>1 : cross-coupling, i.e., a-coefficients not sensitive to s=1 (i.e., „mean“ rotation rate)

Inversion for rotation – first results

$$\Omega(r,\theta) r \sin\theta = -\sum_s w_s(r)\partial_\theta Y_s^0(\theta,\phi)$$

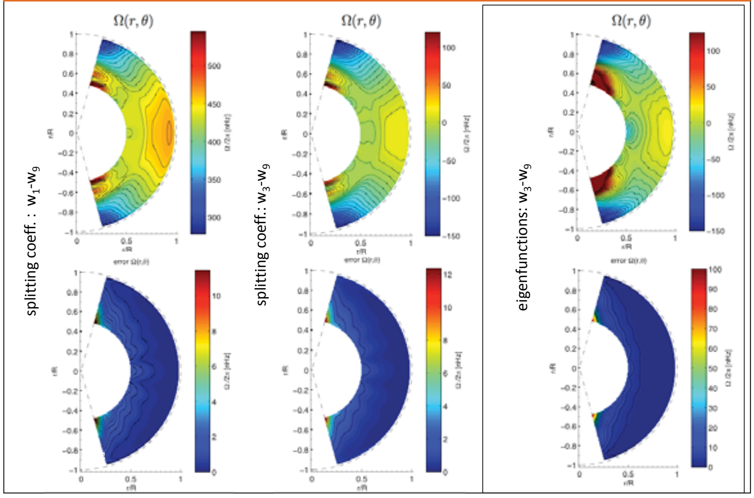

Inversion for rotation – first results

$$\Omega(r,\theta) r \sin\theta = -\sum_s w_s(r)\partial_\theta Y_s^0(\theta,\phi)$$

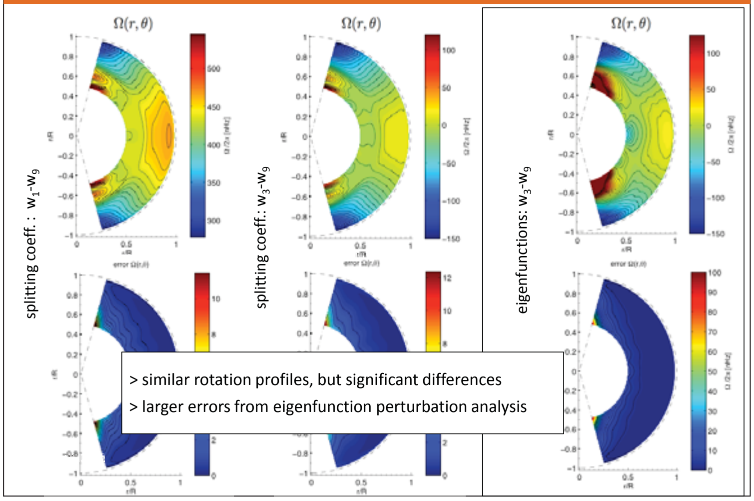

> similar rotation profiles, but significant differences
> larger errors from eigenfunction perturbation analysis

Summary

> analysis of simulated data – resembles flow, differences must be cleared
> rotation profiles are similar, but there are significant differences
> origin so far unclear: - leakage matrix
- numerical: SOLA inversion
- parameter estimation – nonlinear model > bias?
- theoretical eigenfunctions of p modes - how good are they, esp. near the surface ?

> disentangle numerical from solar issues
> test different leakage matrices
> compare different inversion methods (SOLA, RLS,...)
> analyze further data (simulated, HMI)

Thank you for your attention!

Thanks to
Markus Roth, Kiepenheuer-Institut für Sonnenphysik, Freiburg
Jens Timmer, University of Freiburg, Freiburg Center for Data analysis and modeling

MDI data & leakage matrix
Jesper Schou, MDI & HMI team, MPS Göttingen
Tim Larson, MDI & HMI team, Stanford University

Inversion for rotation: comparison of results

> Results for s=2,...,9:
- splitting coeff. (black)
- eigenfun. perturbation (blue)

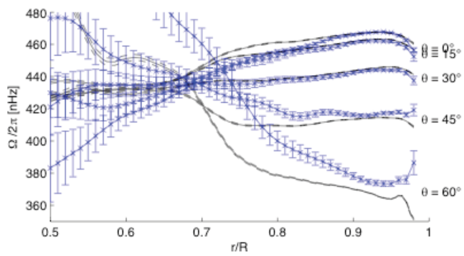

Inversion for rotation

> Results for s=2,...,9:

- splitting coeff. (black)

- eigenfun. perturbation (blue)

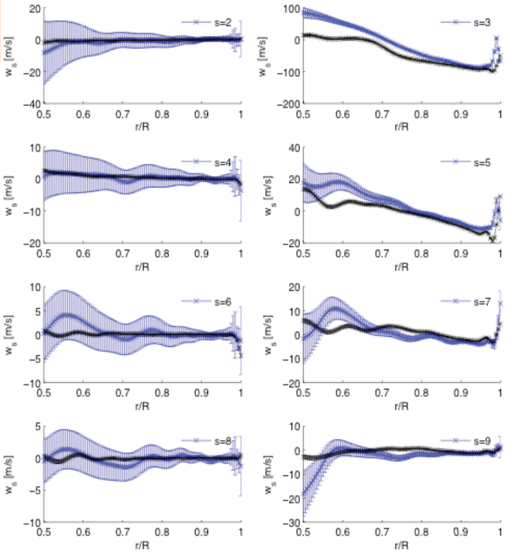

7. Richard Bogart

HMI Local Helioseismology Data: Status and Prospects

Richard Bogart

Stanford University

Local Helioseismology Data Products

series	module	cadence (sec/rec)	size (MB/rec)	Description
hmi.V_avg120	*datavg*	396000	60	1/3 rotation averages of Dopplergrams with orbital velocity removed, for detrending
hmi.rdVtrack_fd05	*mtrack*	12	18	mosaics of tracked mapped data cubes from data in series hmi.V_45s
hmi.rdVtrack_fd15	*mtrack*	340	472	
hmi.rdVtrack_fd30	*mtrack*	2500	1000	
hmi.tdVtrack_synopHC	*mtrack*	993	250	
hmi.rdVpspec_fd05	*pspec3*	12	12	mosaics of the power spectra of the tracked tiles in the series hmi.rdVtrack_fd*, with 1-to-1 mapping of most parameters
hmi.rdVpspec_fd15	*pspec3*	340	324	
hmi.rdVpspec_fd30	*pspec3*	2500	648	
hmi.rdVavgpspec_fd15	*datavg*	8400	324	mosaics of full-rotation averages of power spectra of tracked tiles in series hmi.rdVpspec_fd*
hmi.rdVavgpspec_fd30	*datavg*	34400	648	
hmi.rdVfitsf_fd05	*ringfitf*	12	0.02	mosaics of the "fast" ("dynamics") fits to the power spectra in series hmi.rdVpspec_fd*
hmi.rdVfitsf_fd15	*ringfitf*	340	0.09	
hmi.rdVfitsf_fd30	*ringfitf*	2500	0.2	
hmi.rdVfitsc_fd05	*ringfitc*	12	0.1	mosaics of the "slow" ("structure") fits to the power spectra in series hmi.rdVpspec_fd*
hmi.rdVfitsc_fd15	*ringfitc*	2500	0.7	
hmi.rdVfitsc_fd30	*ringfitc*	10000	0.9	
hmi.tdVtimes_synopHC	*travel_times*	993	22	mosaics of travel time fits to the data in series hmi.tdVtrack_synopHC
hmi.rdVflows_fd15_frame	*rdvinv*	98000	2.25	flow inversions of the fits in all records for a given analysis time in series hmi.rdVfitsf_fd*
hmi.rdVflows_fd30_frame	*rdvinv*	196000	0.57	
hmi.tdVinvrt_synopHC	*invert_td_hr*	248	11	flow and sound-speed inversions of the travel time fits in in series hmi.tdVtimes_synopHC

Tracked Doppler data - common input for *most* local helioseismology analysis

Ring-diagram tiles at three size scales: 32°, 16°, and 5°.12 "squares"

(Uniform apodization to: 30°, 15°, and 5° circles)

Time-distance tiles: 30°.72 "squares"

R-D tile spacings: ~15°, 7°.5, and 2°.5 in arc; T-D tile spacings 24° in latitude and longitude

- R-D Latitude spacing uniform, with tiles centered at 0, ±s, ±2s, ...
- R-D Longitude spacing depends on latitude, same as latitude spacing at equator, and subject to constraint of integer divisor of 360°
- 4 additional T-D tiles at 20° spacings from edges on equator and meridian

Mapping with Postel's projection at scale of 0°.04 / pxl (5° and 15° tiles), 0°.08 / pxl (30° tiles), and 0°.06 / pxl (T-D tiles)

R-D regions tracked while within 80° of disc center

- Three different sets, depending on heliographic latitude of SDO

R-D regions tracked at Carrington rate

- Maximum photospheric zonal velocity 260 m/s at 50°
- Maximum photospheric drift rate 4°.34 / day at poles

T-D regions tracked at nominal photospheric Doppler rate at center of region

Distribution of Ring-diagram Target Regions

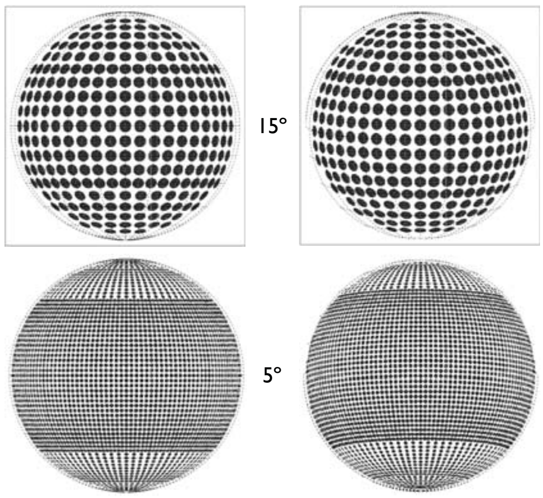

Tracked Doppler data cubes, centred at 2152:210 (2014.07.09_08:45)

5° @ 12.5W07.5S

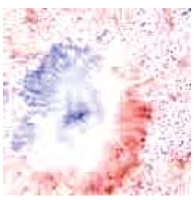

30° @ 15.0W00.0N

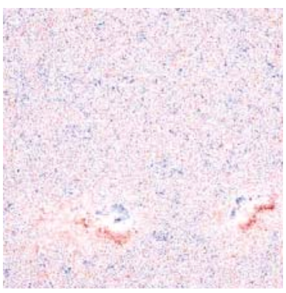

HELAS VI / SOHO 28 / SPACEINN, MPS, Göttingen, 1 September 2014

15° power spectrum, 2151:240 (2014.06.09_21:36), 00.0W00.0N

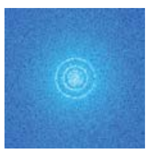

2.5 mHz

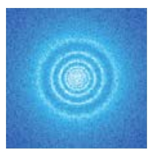

3.5 mHz

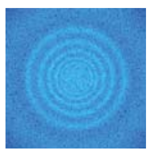

5.0 mHz

HELAS VI / SOHO 28 / SPACEINN, MPS, Göttingen, 1 September 2014

15° power spectrum, 2151:240 (2014.06.09_21:36), 00.0W00.0N

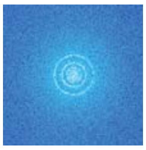
2.5 mHz

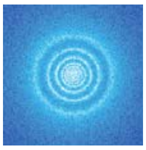
3.5 mHz

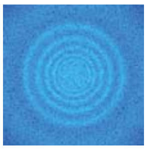
5.0 mHz

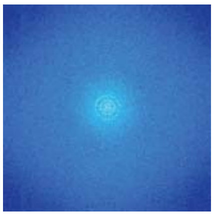

HELAS VI / SOHO 28 / SPACEINN, MPS, Göttingen, 1 September 2014

15° power spectra cuts @ 2.5 mHz around disc

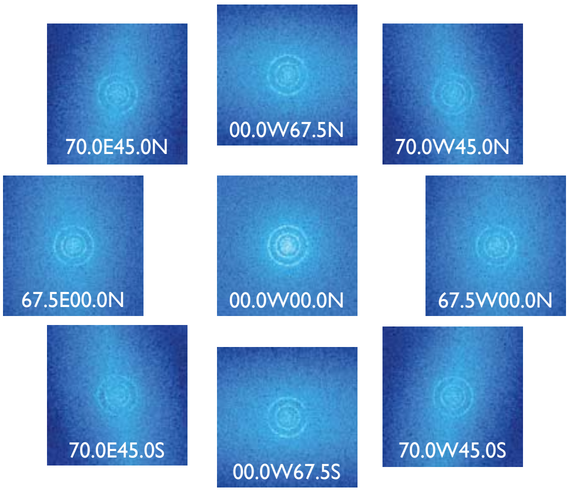

l-ν for ring-diagram fits to power spectra, 2151:240, 00.0W00.0N

5° 15° 30°

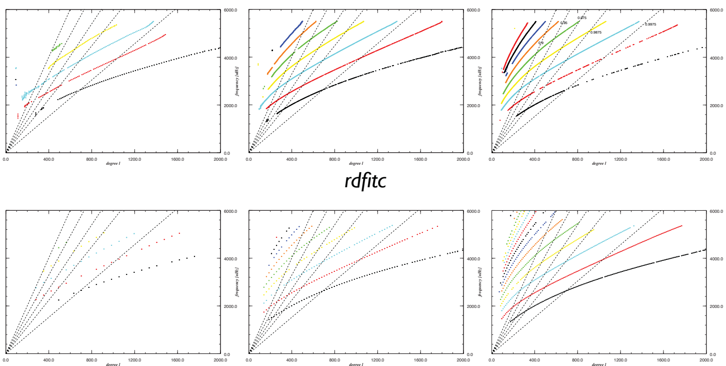

rdfitc

rdfitf

Sample flow inversions over the disc at different depths, 2101:240

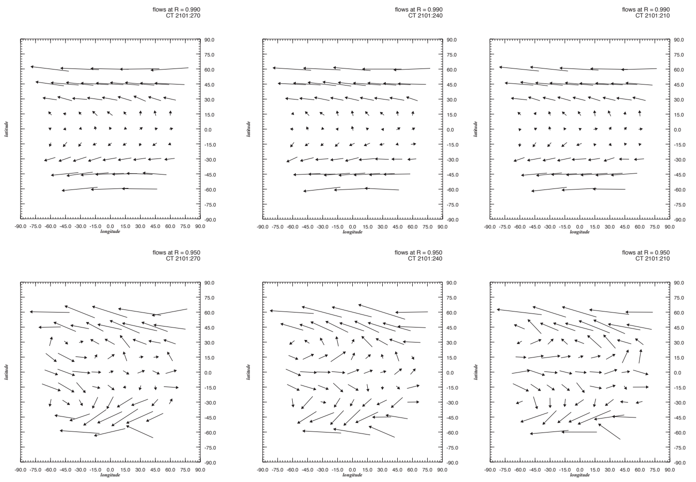

Time-Distance Sound-Speed Inversions

2014.07.09_12:00

Gabor Wavelet

Target Depth [Mm]

Fitting Method

Gizon-Birch

Inversion Method

Born Approx   Ray Path

Time-Distance Sound-Speed Inversions

2014.07.09_12:00

Gabor Wavelet

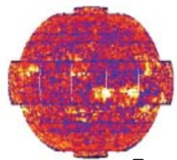
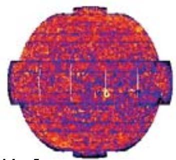

Target Depth [Mm]

Fitting Method

0.5

Gizon-Birch

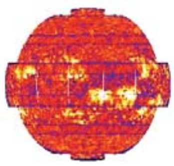
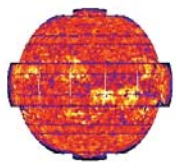

Inversion Method

Born Approx   Ray Path

Ring-diagram Data Products

Delay between Observation and Completion of Processing

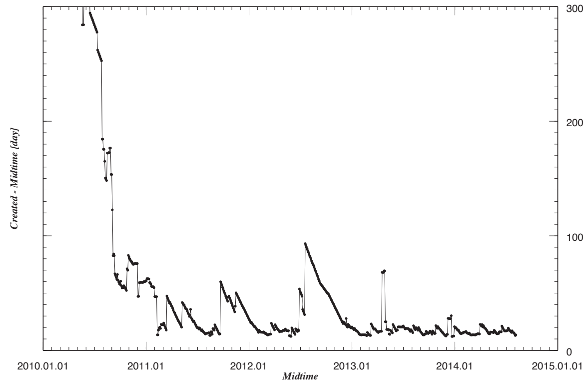

Time-distance Data Products

Delay between Observation and Completion of Processing

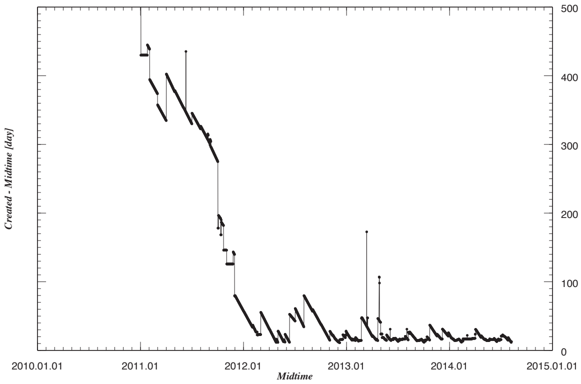

Prospects

More of Same

Identical analysis (almost) applied to MDI, GONG, and Mt Wilson data sets

Ring-Diagrams

Addition of multi-ridge fit code to pipeline

Full-disc fitc fits for 15° tiles

Improved fitting procedures to account for spatial variations

Time-Distance

???

Spatial Distribution of Averaged mode-fit Parameters

n = 1–3, $0.9875 < r_T < 0.9975$

U_x

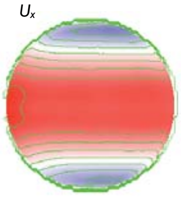

(25 m/s contours)

4-year mean 5° *rdfitc*
CR 2096:250–2149:050
(2010.05.01_02:12–2014.04.30_19:59)

U_y

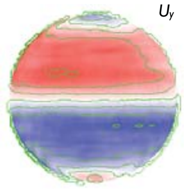

(5 m/s contours)

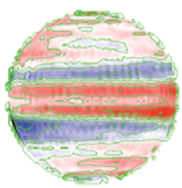

(2.5 m/s contours)

last 2 yrs minus first 2 yrs 5° *rdfitc*
CR 2123:330–2149:050 -
CR 2096:250–2123:335

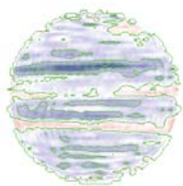

(2.5 m/s contours)

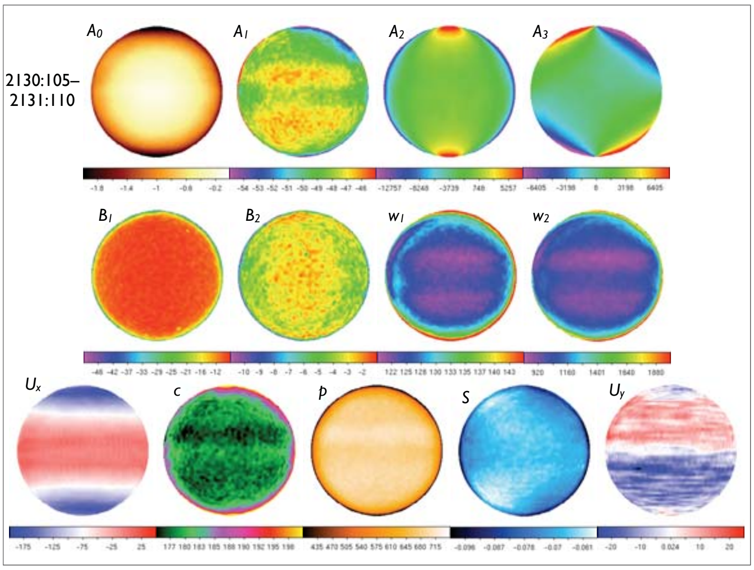

HMI & MDI Coverage during Comparison Interval

2096:240 – 2098:015 (2010 05.01–07.12)

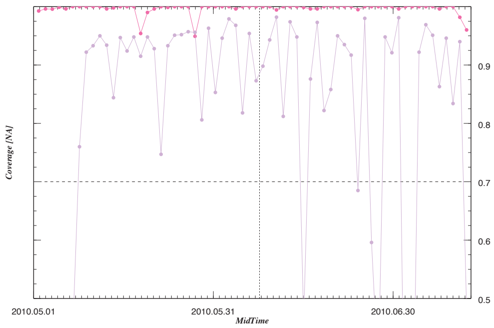

Differences in 4-year means of *rdfitf* and *rdfitc* flow parameters

U_x

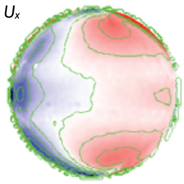

(2.5 m/s contours)

U_y

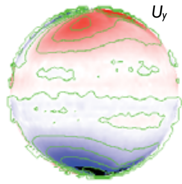

Differences in 2.5-month means of *rdfitm* and *rdfitc* flow parameters (MDI data, 2096:150–2098:030)

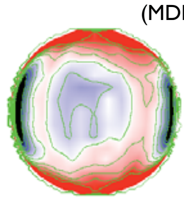

(5 m/s contours)